

Brain Tumor Imaging in Adolescents and Young Adults: 2021 WHO Updates for Molecular-based Tumor Types

Matthias W. Wagner, MD • Pejman Jabejdar Maralani, MD • Julie Bennett, MD • Liana Nobre, MD • Mary Jane Lim-Fat, MD • Peter Dirks, MD, PhD • Suzanne Laughlin, MD • Uri Tabori, MD • Vijay Ramaswamy, MD, PhD • Cynthia Hawkins, MD, PhD • Birgit B. Ertl-Wagner, MD, PhD, MHBA

From the Division of Neuroradiology, Department of Diagnostic Imaging (M.W.W., S.L., B.B.E.W.), Division of Hematology/Oncology (J.B., L.N., U.T., V.R.), Department of Paediatric Laboratory Medicine, Division of Pathology (C.H.), Division of Neurosurgery (P.D.), and Division of Pediatric Neuroradiology (M.W.W.), The Hospital for Sick Children, 555 University Ave, Toronto, ON, Canada M5G 1X8; Neurosciences & Mental Health Research Program, SickKids Research Institute, Toronto, Canada (M.W.W., B.B.E.W.); Department of Medical Imaging, University of Toronto, Toronto, Canada (M.W.W., P.J.M., B.B.E.W.); Department of Diagnostic and Interventional Neuroradiology, University Hospital Augsburg, Augsburg, Germany (M.W.W.); Divisions of Neuroradiology (P.J.M.) and Neurooncology (M.J.L.F.), Sunnybrook Health Science Centre, Toronto, Canada; and Department of Medical Oncology and Hematology, Princess Margaret Cancer Centre, Toronto, Canada (J.B.). Received March 28, 2023; revision requested April 24; revision received November 16; accepted December 1. **Address correspondence to** M.W.W. (email: m.w.wagner@me.com).

Conflicts of interest are listed at the end of this article.

Radiology 2024; 310(2):e230777 • <https://doi.org/10.1148/radiol.230777> • Content codes: **NR** **OI**

Published in 2021, the fifth edition of the World Health Organization (WHO) classification of tumors of the central nervous system (CNS) introduced new molecular criteria for tumor types that commonly occur in either pediatric or adult age groups. Adolescents and young adults (AYAs) are at the intersection of adult and pediatric care, and both pediatric-type and adult-type CNS tumors occur at that age. Mortality rates for AYAs with CNS tumors have increased by 0.6% per year for males and 1% per year for females from 2007 to 2016. To best serve patients, it is crucial that both pediatric and adult radiologists who interpret neuroimages are familiar with the various pediatric- and adult-type brain tumors and their typical imaging morphologic characteristics. Gliomas account for approximately 80% of all malignant CNS tumors in the AYA age group, with the most common types observed being diffuse astrocytic and glioneuronal tumors. Ependymomas and medulloblastomas also occur in the AYA population but are seen less frequently. Importantly, biologic behavior and progression of distinct molecular subgroups of brain tumors differ across ages. This review discusses newly added or revised gliomas in the fifth edition of the CNS WHO classification, as well as other CNS tumor types common in the AYA population.

© RSNA, 2024

Brain and other central nervous system (CNS) tumors remain the second most common tumor type for individuals aged 15–39 years, defined as adolescents and young adults (AYAs) per the Central Brain Tumor Registry of the United States (1), with an incidence rate of 12.21 per 100 000 (1). While overall rates of cancer survival have improved in this population in recent years, mortality rates for AYAs with CNS tumors have increased by 0.6% per year for males and 1% per year for females from 2007 to 2016 (2). The AYA age group represents a unique patient population at the intersection of pediatric and adult care, yet they are considered an understudied population. Indeed, the low participation rate of AYAs in clinical trials has been associated with poorer survival outcomes (2). Symptoms preceding the diagnosis of a brain tumor in AYAs are typically nonspecific; in a case-control study of 899 children and younger adults (age range, 10–24 years), headache was the most frequent symptom across all tumor types (60%) (3). Lack of systematic health care and disregard for nonspecific symptoms in this age group contribute to a prolonged time to diagnosis (4). In the MOBI-Kids study, there was a delay of more than 1 year between onset of first symptoms and diagnosis in nearly 12% (80 of 695) of patients (3). As AYAs are at the intersection of adult and pediatric radiology, brain tumors in this population can occur across different subtypes of adult- and pediatric-type gliomas,

medulloblastomas, and ependymomas (5). The most common brain tumors in AYA patients are diffuse astrocytic and oligodendroglial tumors, glioneuronal tumors, ependymal tumors, other gliomas, and medulloblastomas. Germ cell tumors, tumors of the choroid plexus, and tumors of the pineal region are less frequently encountered (1). The unique biology of brain tumors in AYAs is reflected in the fifth edition of the World Health Organization (WHO) classification of tumors of the central nervous system (hereafter, CNS WHO) (6).

Radiologists are integral in the diagnosis and management of patients with brain tumors. As such, familiarity with the fifth edition of the CNS WHO tumor classification (6), as well as knowledge of principles of molecular characterization and tumor-specific imaging morphologic characteristics, are important. Research in brain tumor biology is rapidly advancing our understanding of these entities, and radiologists are challenged to adopt new nomenclatures and classification systems and to understand underlying tumor biology and behavior.

This review discusses updates to the 2021 CNS WHO tumor classification, with a focus on molecular and imaging characteristics of relevant tumor types common in AYAs. Tables 1 and 2 summarize abbreviations commonly used in the classification and molecular description of tumors and provide information about their imaging features and clinical significance.

Abbreviations

AYA = adolescent and young adult, CNS = central nervous system, FLAIR = fluid-attenuated inversion recovery, IDH = isocitrate dehydrogenase, MAPK = mitogen-activated protein kinase, SHH = sonic hedgehog, WHO = World Health Organization, WNT = wingless type



Summary

Familiarity with specific imaging morphologic characteristics of pediatric- and adult-type tumors of the central nervous system is essential to provide the best imaging care to adolescents and young adults as both tumor types can occur in this age group.

Essentials

- As adolescents and young adults (AYAs) are at a transitional phase between adult and pediatric care, it is important for radiologists to recognize that central nervous system (CNS) tumors in this age group can include various subtypes of either adult- or pediatric-type gliomas, medulloblastomas, and ependymomas.
- Gliomas account for approximately 80% of all malignant CNS tumors in AYA patients.
- For ependymomas and medulloblastomas, biologic behavior and prognosis differ according to patient age.

Glioma

In the AYA age group, gliomas account for approximately 80% of all malignant CNS tumors (1). Adult- and pediatric-type gliomas, circumscribed astrocytic gliomas, and glioneuronal and neuronal tumors can all occur in the AYA population. Of note, despite the terms “adult-type” and “pediatric-type,” these tumors can be encountered throughout the AYA age span, and it is important that both pediatric and adult neuroradiologists are familiar with both categories (5). Two radiologic flowcharts (Figs 1, 2) can aid in the diagnosis of pediatric-type gliomas.

Adult-type Diffuse Glioma

Astrocytoma, Isocitrate Dehydrogenase–Mutant

In the fifth edition of the CNS WHO classification, isocitrate dehydrogenase (IDH)–mutant astrocytoma is defined as a diffusely infiltrating glioma with *IDH1* or *IDH2* mutation and absence of 1p/19q codeletion. Furthermore, these tumors typically exhibit loss of nuclear *ATRX* expression and harbor *TP53* mutations. Astrocytomas with IDH mutations are now graded 2–4, and the term glioblastoma is no longer applied to these gliomas (6).

Specific MRI features can be used to help identify IDH-mutant astrocytoma. One such imaging finding is the T2-weighted fluid-attenuated inversion-recovery (FLAIR) (hereafter, T2/FLAIR) mismatch sign, defined as having hyperintense signal with T2-weighted sequences and hypointense signal with FLAIR sequences, with a hyperintense peripheral rim (7). Appearance of this mismatch sign on MRI scans has been found to be highly specific (100%) and moderately sensitive (40%) for IDH-mutant astrocytoma (8,9). Other characteristic imaging features include peritumoral signal abnormality and contrast

enhancement, which are more commonly encountered in CNS WHO grade 3 and 4 tumors. As IDH-mutant astrocytomas are designated CNS WHO grade 4 based on *CDKN2A/B* homozygous deletion, no reliable imaging features exist to differentiate this tumor entity from a lower-grade IDH-mutant astrocytoma (Fig 3) (10,11). The main differential diagnoses of IDH-mutant astrocytoma in the AYA age group are glioblastoma and oligodendroglioma. Presence of contrast enhancement can be helpful in differentiating glioblastomas from low-grade astrocytomas and low-grade oligodendrogliomas. A key feature of oligodendrogliomas are coarse calcifications, which are less common in IDH-mutant astrocytoma and glioblastoma.

Oligodendroglioma, IDH-Mutant and 1p/19q-Codeleted

Oligodendroglioma is defined as diffusely infiltrating tumor with an IDH mutation and 1p/19q-codeletion. Grading (CNS WHO 2 or 3) is based on the histologic assessment of mitotic activity, necrosis, and microvascular proliferation. Homozygous deletion of *CDKN2A/B* upgrades the tumor to CNS WHO grade 3, independent of histologic findings (6). Approximately 50%–65% of oligodendrogliomas occur in the frontal lobe; they are less frequently encountered in the occipital and parietal lobes (12,13).

Oligodendrogliomas are typically located in the cortex and/or subcortical white matter. Compared with IDH-mutant astrocytomas, oligodendrogliomas are less well circumscribed and demonstrate a higher degree of internal heterogeneity and edema (Fig 4). Compared with 1p/19q-intact gliomas, intratumoral calcifications are moderately sensitive (51%) and highly specific (91%) for IDH-mutant and 1p/19q-codeleted oligodendrogliomas (14). Contrast enhancement occurs in 46% of oligodendrogliomas and is more frequently encountered in CNS WHO grade 3 than grade 2 oligodendrogliomas (15). As defined by the 2016 CNS WHO classification of tumors (16), oligodendrogliomas have higher relative cerebral blood volume and higher cellular density than astrocytomas (17).

Glioblastoma, IDH–Wild Type

In the fifth edition of the CNS WHO classification, the term *glioblastoma* is now restricted to high-grade diffuse gliomas, which are IDH–wild type and histone protein H3–wild type. Diagnosis of this tumor type is based on morphologic findings of a diffuse glioma with increased mitotic activity and microvascular proliferation and/or pseudopalisading necrosis, as well as molecular findings that include *TERT* promoter mutation, *EGFR* amplification, or combined gain of whole chromosome 7 and loss of chromosome 10 (+7/–10) (6).

At the time of diagnosis, glioblastomas are often large tumors demonstrating thick and irregular contrast enhancement at the tumor margin on MRI scans. Necrosis with or without a hemorrhagic component can be seen in the tumor core. FLAIR images typically demonstrate perilesional hyperintense signal, which usually represents neoplastic infiltration (10,11). Besides IDH-mutant high-grade astrocytoma, cerebral metastases and primary CNS lymphoma with central necrosis in the context of AIDS may appear very similar to glioblastoma at imaging. Cerebral abscesses and tumefactive demyelination are important nonneoplastic differential diagnoses.

Table 1: Abbreviations, Typical Locations, and Key Imaging Features for Tumors of the Central Nervous System Commonly Encountered in Adolescents and Young Adults

Abbreviation	Tumor Entity	Typical Location	Key Imaging Feature
DMG	Diffuse midline glioma	Midline; pontine variant is classic; if midbrain or medulla, also consider WHO grade 1 or 2	Pontine: most often no enhancement or diffusion restriction, engulfing basilar artery; WHO grade 1 or 2: focal and/or dorsally exophytic
DNET	Dysembryoplastic neuroepithelial tumor	Cortical	Multicystic with “bubbly appearance,” faint enhancement and calcification is possible
HGAP	High-grade astrocytoma with piloid features	Cerebellum	Limited studies; sharp or diffuse margin, rim or patchy enhancement, no diffusion restriction
HGG	High-grade glioma	Hemispheric or midline	Hemispheric: well delineated or diffusely infiltrative and multifocal or monocentric, with absent or intense enhancement, ependymal/leptomeningeal contact; midline: see above
JPA	Juvenile pilocytic astrocytoma	Cerebellum is classic; optic pathway in neurofibromatosis type 1	Large cystic tumor with small enhancing mural nodule
LGG	Low-grade glioma	Hemispheric, cerebellar	Diverse imaging features
MVNT	Multinodular and vacuolating neuronal tumor	Sub- and juxtacortical	Multiple small T2/fluid-attenuated inversion-recovery hyperintense nodules without mass effect
PFA	Posterior fossa group A ependymoma	Likely to arise from roof or lateral portions of fourth ventricle	Classic is extension through the foramina of Luschka and Magendie; calcification more common than in posterior fossa group B
PFB	Posterior fossa group B ependymoma	Frequently arises from fourth ventricular floor	Classic is extension through the foramina of Luschka and Magendie, cyst formation; larger enhancing tumor component than posterior fossa group A
pLGG	Pediatric low-grade glioma	Hemispheric, cerebellar	Facilitated diffusion, diverse imaging features
PLNTY	Polymorphous low-grade neuroepithelial tumor of the young	Temporal lobe, right to left, cortical and subcortical	Solid with peripheral cystic components, no or mild enhancement, central coarse calcification
PXA	Pleomorphic xanthoastrocytoma	Cortical	Solid enhancing nodule, peripheral cystic component, scalloping, possibly dural tail sign
SHH-MB	Sonic hedgehog–activated medulloblastoma	Cerebellar hemispheres	Solid enhancement more common than other groups, hemorrhage
STE	Supratentorial ependymoma	Frontal and parietal lobes	Cystic, solid component with diffusion restriction and enhancement, peritumoral edema and internal hemorrhage

Note.—WHO = World Health Organization.

Pediatric-type Diffuse Glioma

Low-grade Glioma, IDH–Wild Type

This new tumor type has been added to the 2021 CNS WHO classification. The four entities of (a) mitogen-activated protein kinase (MAPK) pathway–altered diffuse glioma, (b) *MYB*- or *MYBL1*-altered diffuse glioma, (c) angiocentric glioma, and (d) polymorphous low-grade neuroepithelial tumor of the young, or PLNTY, all feature diffuse tumor growth but are expected to behave less aggressively than pediatric-type diffuse high-grade gliomas (6).

Genetic alterations in diffuse glioma, MAPK pathway–altered tumors, include duplication of the *FGFR1* tyrosine kinase domain, other *FGFR1* mutations, and *BRAF* mutations that lead to the amino acid substitution V600E in the BRAF protein (p. V600E), among others (18). Further criteria are the

absence of IDH and histone H3 mutations and homozygous deletion of *CDKN2A* (11).

Imaging features are not well described at present (19) but likely vary depending on the underlying molecular alteration. The MRI features of a diffuse glioma with *MAP2K1* gene mutation are shown in Figure 5.

MYB- or *MYBL1*-altered diffuse astrocytomas are rare CNS WHO grade 1 tumors. The *MYB* and *MYBL1* genes serve as transcriptional regulators important for cell proliferation and differentiation. These tumors are typically found in a cortical and subcortical location and are more commonly encountered in the cerebral hemispheres than in the diencephalon or brainstem (20).

Features on MRI scans include T1-weighted isointensity to hypointensity, T2/FLAIR mixed signal intensity or hyperintensity compared with cortex, and absence of diffusion restriction. In a case series of 23 patients, only one patient showed faint

Table 2: Molecular Markers with Clinical Significance in Tumors of the Central Nervous System Commonly Encountered in Adolescents and Young Adults

Gene Symbol	Gene Name	Clinical Significance
<i>IDH1/2</i>	Isocitrate dehydrogenase (NADP ⁺) 1/2	If mutated, better prognosis and longer survival compared with tumors without these mutations
<i>TP53</i>	Tumor protein P53	If mutated, more aggressive tumor behavior and worse prognosis
<i>CDKN2A/B</i>	Cyclin-dependent kinase inhibitor 2A/2B	Associated with poor prognosis when homozygous deletion is present in astrocytoma, isocitrate dehydrogenase–mutant
<i>EGFR</i>	Epidermal growth factor receptor	Associated with increased tumor growth and poor prognosis if amplified
<i>MAPK</i>	Mitogen-activated protein kinase	Involved in regulating cell growth and survival; aberrant activation is identified in various brain tumors, contributing to tumor progression and resistance to therapy
<i>MYB</i>	MYB proto-oncogene, transcription factor	Mandatory for the newly recognized <i>MYB</i> - or <i>MYBL1</i> -altered diffuse astrocytoma; <i>MYB-QKI</i> fusion in 80%–90% of angiocentric gliomas
<i>TERT</i>	Telomerase reverse transcriptase	Mutations and rearrangements associated with worse prognosis and more aggressive behavior
<i>FGFR1/2/3</i>	Fibroblast growth factor receptor 1/2/3	Diagnostic and prognostic markers
<i>PRKCA</i>	Protein kinase C alpha	Overexpression may contribute to tumor growth and progression; present in 80%–90% of chordoid gliomas
<i>ZFTA</i>	Zinc finger translocation-associated	Most frequent recurrent genetic alteration in supratentorial ependymomas
<i>YAP1</i>	Yes1-associated transcriptional regulator	Overexpression or activation can promote cell proliferation and inhibit apoptosis

Note.—NADP⁺ = nicotinamide adenine dinucleotide phosphate.

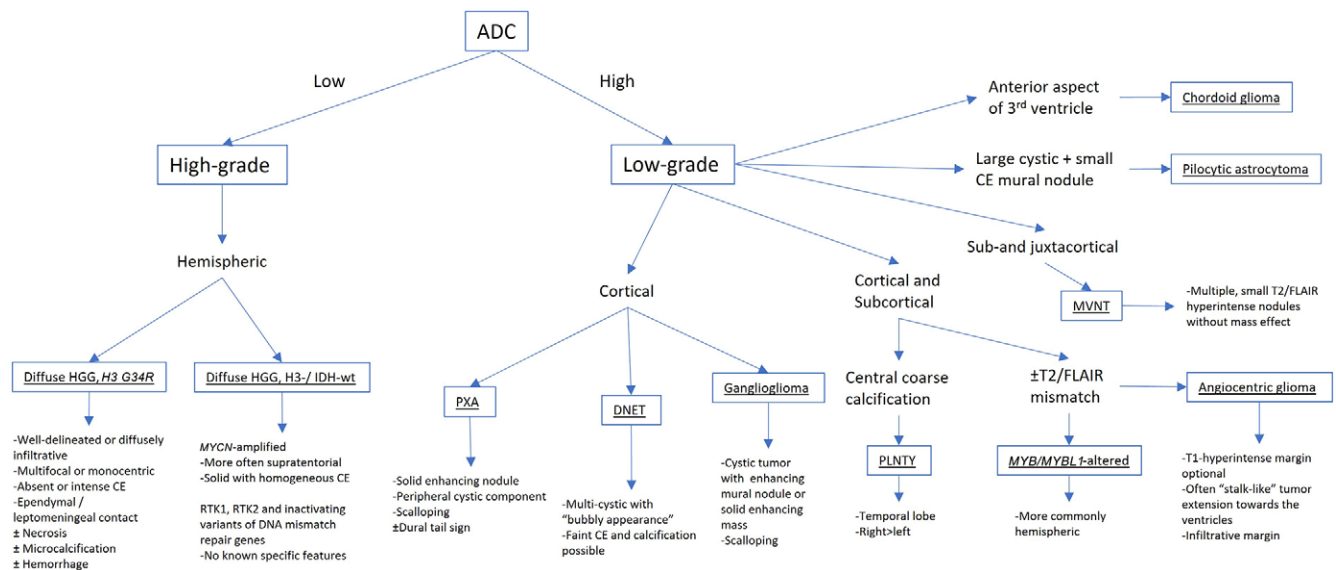


Figure 1: Radiologic flowchart of pediatric low-grade gliomas and hemispheric high-grade gliomas (HGG) based on apparent diffusion coefficient (ADC) map values, anatomic location, and MRI signal characteristics. Mitogen-activated protein kinase pathway–altered diffuse gliomas are not included due to the scarcity of reported imaging findings. Also not included are high-grade astrocytomas with piloid features, which demonstrate rim enhancement with a lack of central enhancement and with increased central apparent diffusion coefficient values (48), as well as astroblastomas with *MN1* alterations, which demonstrate heterogeneous contrast enhancement, abundant susceptibility artifacts due to hemorrhage and/or calcification, and diffusion restriction of the solid tumor component (30). CE = contrast enhancement, DNET = dysembryoplastic neuroepithelial tumor, FLAIR = fluid-attenuated inversion recovery, IDH = isocitrate dehydrogenase, MVNT = multinodular and vacuolating neuronal tumor, PLNTY = polymorphous low-grade neuroepithelial tumor of the young, PXA = pleomorphic xanthoastrocytoma, RTK = receptor tyrosine kinase, T2 = T2-weighted, wt = wild type.

diffuse contrast enhancement (21). Tumors are usually well circumscribed and may have cystic portions. Microcystic tumor components may give rise to a T2/FLAIR mismatch sign, which has been occasionally observed on MRI scans of diffuse astrocytoma with *MYB/MYBL1* alteration (Fig 6) (9,22,23).

Angiocentric gliomas are rare CNS WHO grade 1 tumors characterized by *MYB* gene alterations, with approximately 80%–90% of these tumors exhibiting *MYB-QKI* gene fusion (20). Angiocentric gliomas are typically focal tumors with infiltrative margins in the supratentorial brain.

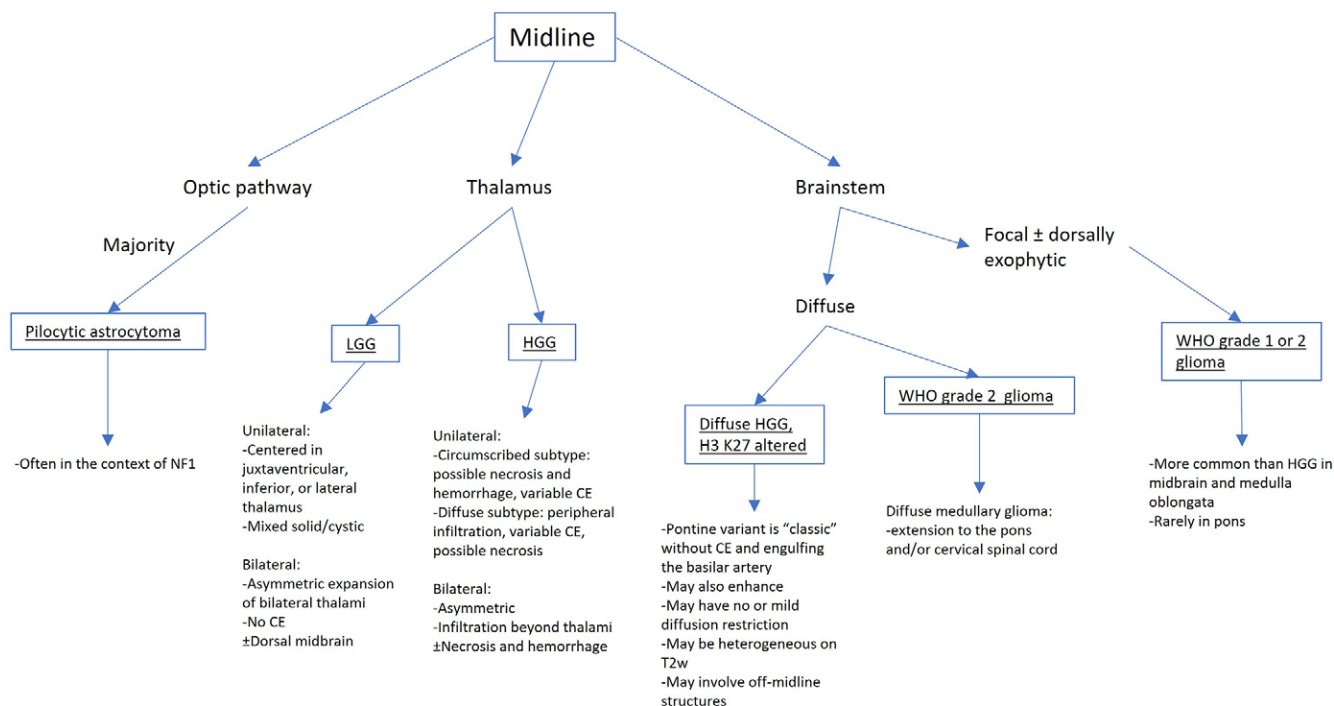


Figure 2: Radiologic flowchart of pediatric midline low-grade glioma (LGG) and high-grade glioma (HGG) based on anatomic location and MRI signal characteristics. CE = contrast enhancement, NF1 = neurofibromatosis type 1, T2w = T2-weighted, WHO = World Health Organization.

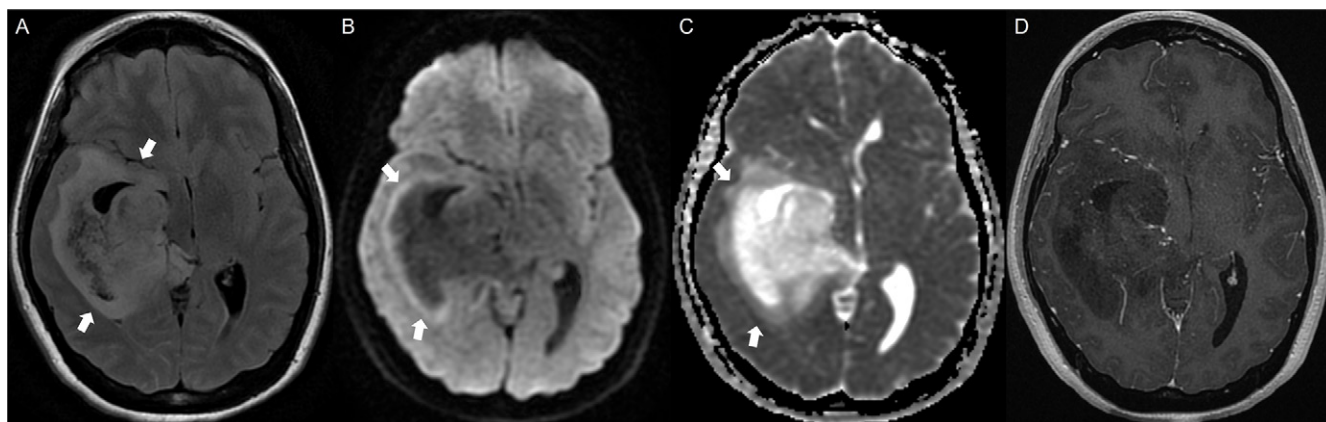


Figure 3: Brain MRI scans in a 30-year-old female patient with isocitrate dehydrogenase-mutant astrocytoma centered in the basal ganglia and right temporal lobe. **(A)** Axial fluid-attenuated inversion-recovery (FLAIR) image shows a heterogeneously hyperintense mass lesion with perilesional edema (arrows). **(B, C)** Axial diffusion-weighted image **(B)** and apparent diffusion coefficient map **(C)** show peripheral diffusion restriction (arrows). **(D)** Axial contrast-enhanced T1-weighted image shows that the tumor does not enhance after contrast administration. The T2/FLAIR mismatch sign (T2-weighted hyperintense appearance of the tumor with corresponding FLAIR hypointensity except for a rim of FLAIR hyperintensity at the tumor margin), which can be observed at MRI for this tumor type, was not present in this patient.

At MRI, angiocentric gliomas are usually T2/FLAIR hyperintense (Fig 7A, 7B) with or without an intrinsically T1-hyperintense margin (Fig 7C). Facilitated diffusivity and absence of contrast enhancement are also common. A “stalk-like” tumor extension toward the ventricles has been described in the majority of patients (Fig 7C) (24,25). The T2/FLAIR imaging appearance resembles that of other pediatric low-grade gliomas and nonneoplastic lesions such as encephalomalacia, cortical laminar necrosis, and gliosis. The tumor-related mass effect, patient history, and stalk-like

tumor extension toward the lateral ventricles usually point toward an angiocentric glioma compared with encephalomalacia. Also, signal abnormalities, such as intrinsic T1 hyperintensity, are usually not as gyriform in angiocentric gliomas as they would be in cortical laminar necrosis.

Polymorphous low-grade neuroepithelial tumor of the young comprises a group of neoplasms designated CNS WHO grade 1, with histologic characteristics of infiltrative growth, oligodendroglioma-like components, calcifications, and aberrant *CD34* expression (26,27). Most are found in a cortical or subcortical

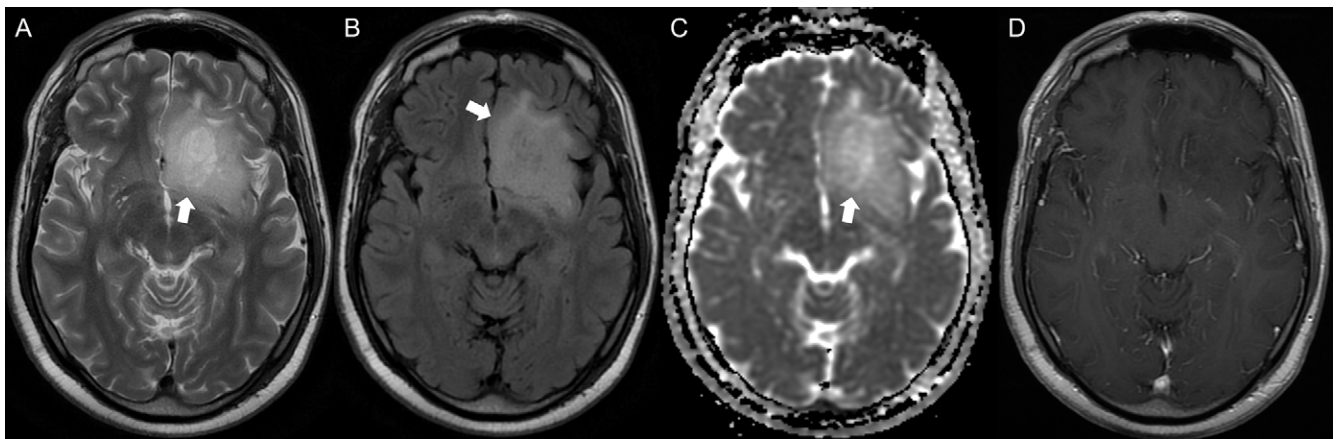


Figure 4: Brain MRI scans in a 36-year-old male patient with isocitrate dehydrogenase–mutant, 1p/19q–codeleted left fronto-insular oligodendroglioma. **(A)** Axial T2-weighted image shows a hyperintense tumor (arrow) with mild midline distortion. **(B)** Axial fluid-attenuated inversion-recovery image shows mild mass effect and indistinct tumor borders (arrow). **(C)** Axial apparent diffusion coefficient map shows facilitated diffusivity (arrow). **(D)** Axial T1-weighted contrast-enhanced image shows absent enhancement following contrast administration.

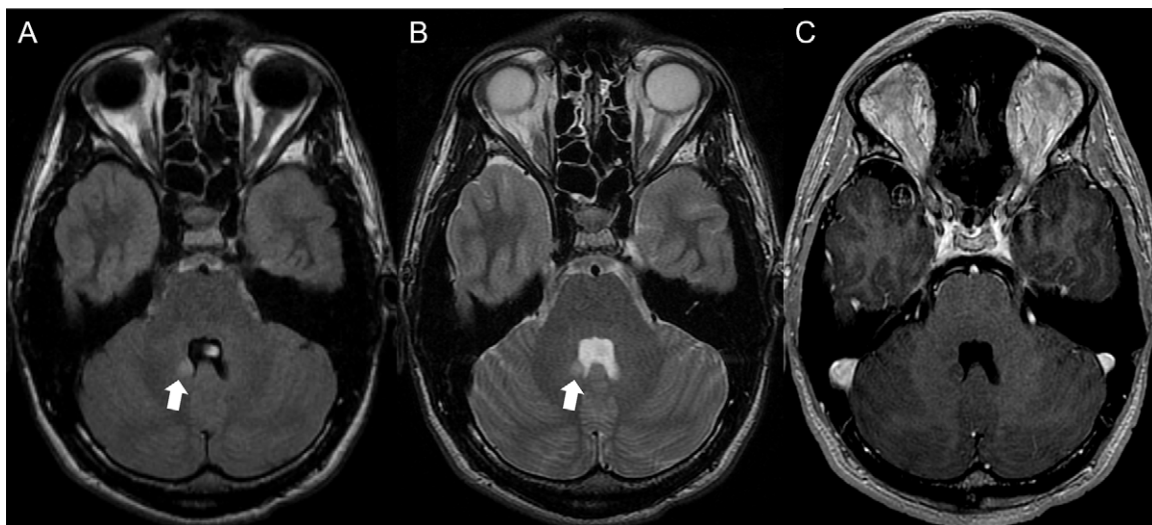


Figure 5: Brain MRI scans in a 16-year-old male patient with a small right cerebellar diffuse astrocytoma with *MAP2K1* gene mutation. **(A)** Axial fluid-attenuated inversion-recovery image shows a hyperintense well-delineated lesion in the right cerebellar periventricular white matter (arrow). **(B)** Axial T2-weighted image shows mild mass effect on the lateral recess of the fourth ventricle (arrow). **(C)** Contrast-enhanced T1-weighted image shows absence of contrast enhancement.

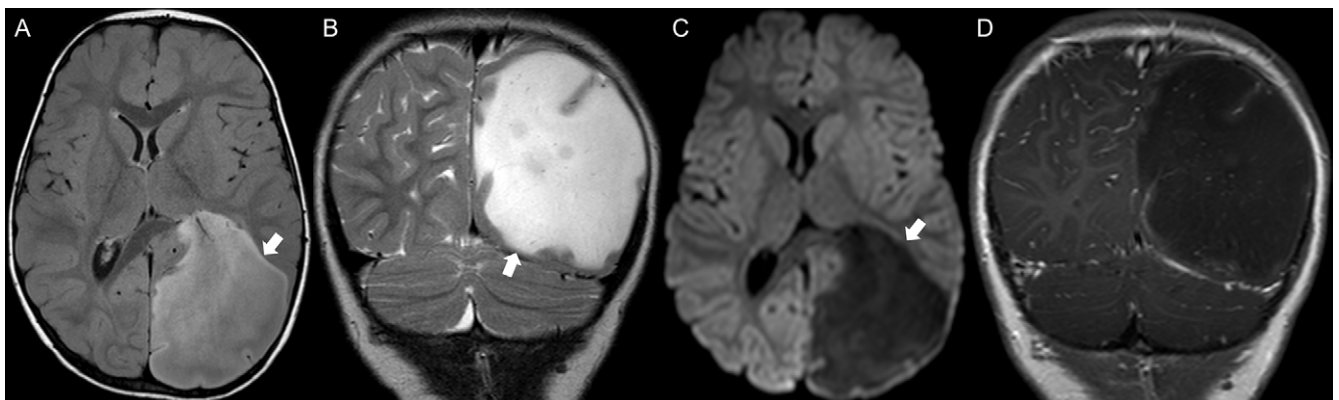


Figure 6: Brain MRI scans in a 2-year-old male patient with a left parieto-occipital diffuse astrocytoma and *MYBL1* alteration. **(A)** Axial T2-weighted fluid-attenuated inversion-recovery (FLAIR) image shows a well-delineated large tumor with central hypointense signal (arrow). **(B)** Coronal T2-weighted image shows hyperintense signal of the tumor in keeping with a “false-positive” T2/FLAIR mismatch sign (arrow). **(C)** Axial diffusion-weighted image does not show restricted diffusion (arrow). **(D)** Coronal contrast-enhanced T1-weighted image shows absence of contrast enhancement of the tumor.

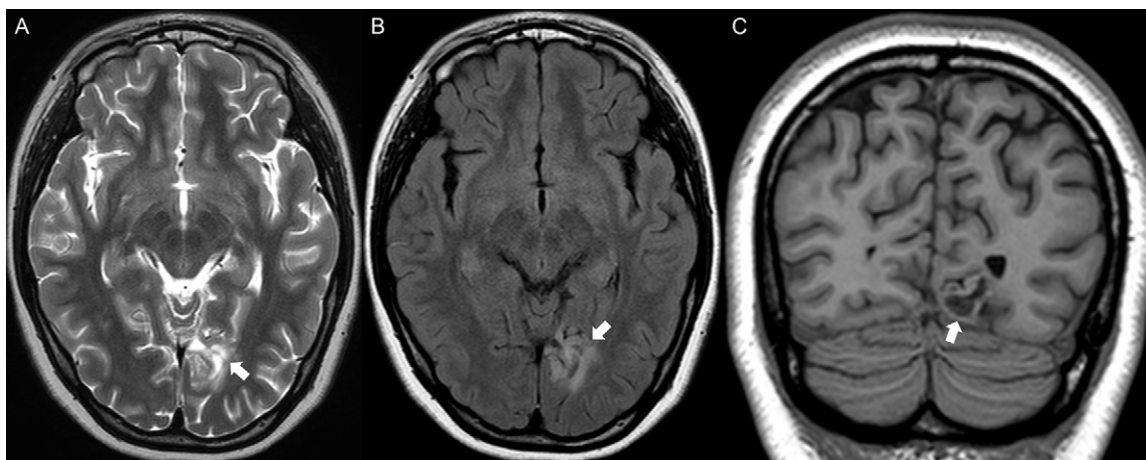


Figure 7: Brain MRI scans in a 16-year-old female patient with left mesial occipital angiocentric glioma with *MYB* alteration. **(A)** Axial T2-weighted image shows a hyperintense tumor (arrow). **(B)** Axial fluid-attenuated inversion-recovery image shows hyperintensity and an irregular shape of the tumor (arrow). **(C)** Coronal T1-weighted image shows a “stalk-like” tumor extension toward the left occipital horn (arrow).

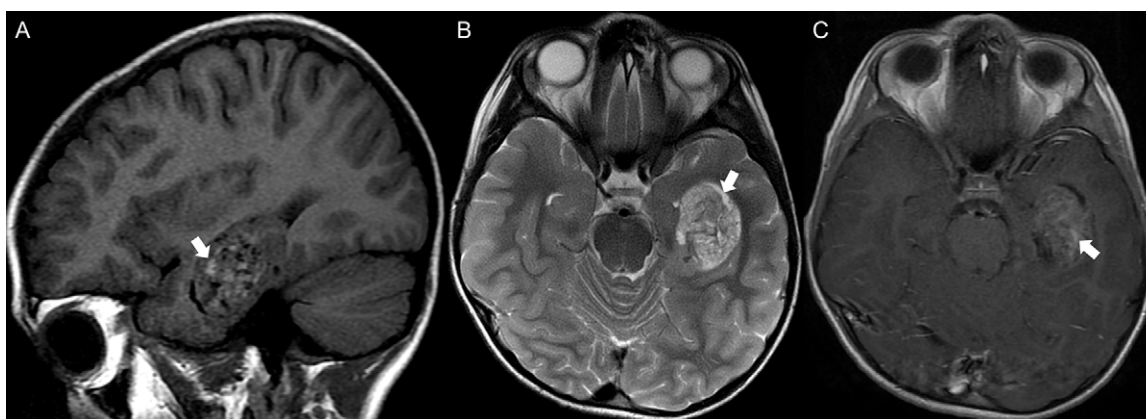


Figure 8: Brain MRI scans in a 7-year-old male patient with left temporal polymorphous low-grade neuroepithelial tumor of the young and *FGFR2* fusion. **(A)** Sagittal T1-weighted image shows intrinsic hyperintense signal suggesting calcification (arrow). **(B)** Axial T2-weighted image shows small peripheral hyperintense cystic components (arrow). **(C)** Axial contrast-enhanced T1-weighted image shows faint enhancement (arrow).

location in the cerebral hemispheres, with a predilection for the temporal lobe (right to left) (28). The mean age at presentation is 18 years (range, 4–32 years) (29).

Polymorphous low-grade neuroepithelial tumors of the young are typically solid with peripheral cystic components. The dominant imaging feature is central coarse calcification (Fig 8A) (27,28). They appear hyperintense with T2-weighted sequences (Fig 8B) and have mild or no contrast enhancement (Fig 8C). This imaging appearance should be differentiated from the more commonly encountered gyriform calcification in oligodendroglioma (29) and from *MNI*-altered astroblastomas, where susceptibility-weighted imaging is reported to show more abundant susceptibility artifacts due to hemorrhage and/or calcification (30).

Diffuse High-grade Glioma, Hemispheric

Diffuse hemispheric H3 G34-mutant glioma is a new tumor type described in the fifth edition of the CNS WHO classification. This tumor entity is designated as CNS WHO grade 4 and characterized by a missense mutation at position 34 of the histone H3.3 protein and absence of IDH mutation (6). This is an

aggressively infiltrating tumor generally encountered in the cerebral hemispheres with possible extension to midline structures. While H3 G34-mutant diffuse hemispheric gliomas account for less than 1% of all gliomas, they account for 13% of high-grade gliomas in the AYA population (31,32).

Imaging characteristics are variable. Tumors are reported to be well delineated or diffusely infiltrative (Fig 9A) and multifocal or monocentric with possible necrosis (Fig 9B), microcalcification, or hemorrhage (Fig 9D). Contrast enhancement ranges from absent to intense. These tumors commonly exhibit restricted diffusion (Fig 9C) and increased perfusion. Contact to the leptomeninges or ependymal margins (Fig 9A, 9B) has been reported in most diffuse high-grade gliomas (33–36). There are no specific imaging features allowing a differentiation of this tumor from H3-wild-type and IDH-wild-type diffuse pediatric-type high-grade glioma.

Diffuse High-grade Glioma, Midline

Diffuse midline gliomas are now designated as H3 K27-altered rather than H3 K27M-mutant to encompass newly discovered

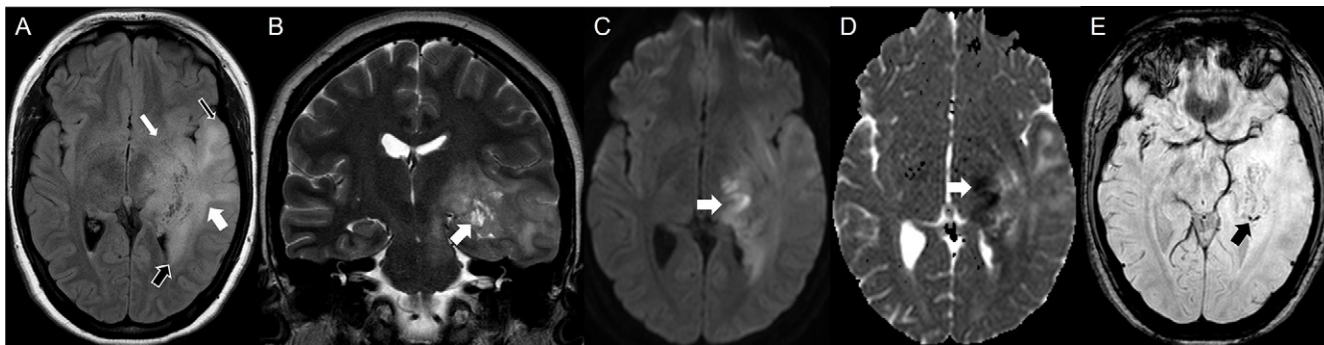


Figure 9: Brain MRI scans in a 17-year-old female patient with diffuse left hemispheric high-grade glioma with a G34R amino acid substitution in the histone H3.3 protein. **(A)** Axial fluid-attenuated inversion-recovery image shows a hyperintense tumor with partially well-delineated (thick white arrow) and partially diffusely infiltrating borders (thin white arrow), with contact to the leptomeninges (thin black arrow) and ependymal margins (thick black arrow). **(B)** Coronal T2-weighted image shows multiple small cysts (arrow). **(C, D)** Axial diffusion-weighted image **(C)** and apparent diffusion coefficient map **(D)** show restricted diffusion along the medial tumor edge (arrow). **(E)** Axial multiplanar gradient-recalled image shows coarse and stippled susceptibility artifacts suggesting microcalcification or hemorrhage (arrow).

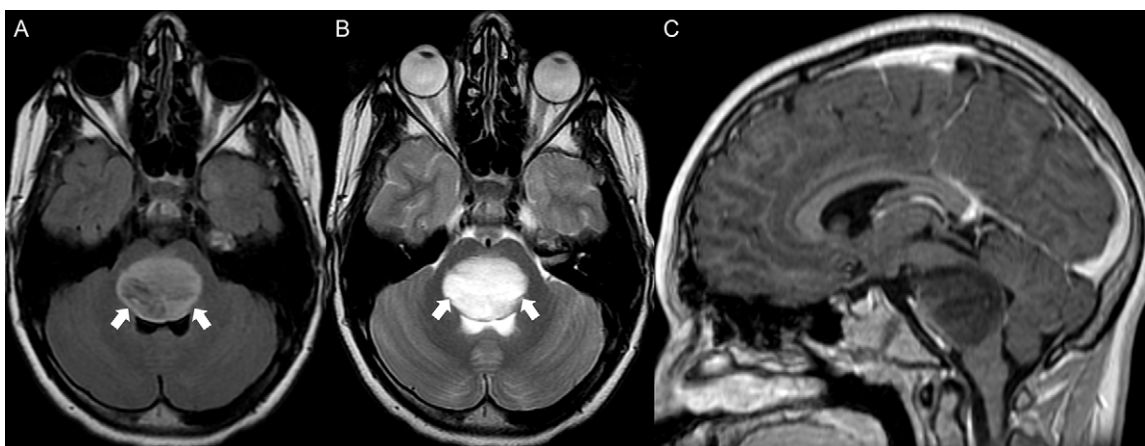


Figure 10: Brain MRI scans in an 11-year-old male patient with diffuse midline high-grade glioma with a K27M amino acid substitution in the histone H3.3 protein. **(A)** Axial fluid-attenuated inversion-recovery image shows a large heterogeneously hyperintense mass lesion (arrows). **(B)** Axial T2-weighted image shows that the lesion is well delineated and hyperintense (arrows). **(C)** Sagittal contrast-enhanced T1-weighted image shows the absence of contrast enhancement.

sequence variants driving the loss of histone H3 K27 trimethylation (37). Regardless of the underlying mechanism, loss of H3 K27 trimethylation is the hallmark feature of these CNS WHO grade 4 tumors. In children, these tumors are most frequently encountered in the pons, but in the AYA age range, thalamic and spinal locations become more frequent (32). Rarely, tumors are found off the midline. Bilateral thalamic tumors most commonly represent the *EGFR*-altered subtype (37,38).

Features observed with MRI are variable without a unifying pattern. The classic appearance of the pontine variant (diffuse intrinsic pontine glioma) is an expansile T2-hyperintense mass lesion centered in the pons (Fig 10A) with or without mild diffusion restriction, engulfing the basilar artery, with pontine fiber splitting (Fig 10B), and without contrast enhancement (Fig 10C). However, diffuse midline gliomas may also appear as enhancing (Fig 11B) and necrotic tumors with heterogeneous T2-weighted signal (Fig 11A) and involve off-midline structures. The differential diagnosis includes focal and dorsally exophytic tumors of the brainstem, which are more commonly found in the midbrain and medulla oblongata, and which are usually low-grade gliomas (39).

Diffuse Pediatric-type High-grade Glioma, H3–Wild Type and IDH–Wild Type

These newly recognized CNS WHO grade 4 tumors are a heterogeneous group with mostly high-grade histologic features (high mitotic activity, vascular proliferation, and/or necrosis). They are defined by the absence of mutations in either IDH or histone 3. There are three molecular subgroups that include *MYCN*-amplified gliomas, RTK1 gliomas (exhibiting *PDGFRA* amplification), and RTK2 gliomas (exhibiting *EGFR* amplification) (6,40,41). Hypermutant diffuse high-grade gliomas have also been observed in children and are characterized by microsatellite instability, which is related to inactivating variants of DNA mismatch repair genes (41).

At imaging, *MYCN*-amplified diffuse high-grade gliomas are more commonly found in the supratentorial brain as a solid lesion with mild to moderate perilesional T2/FLAIR hyperintense signal, relatively homogeneous contrast enhancement (Fig 12A–12D), restricted diffusion in the solid part of the tumor due to hypercellularity (Fig 12E, 12F), and higher perfusion (42). There are no specific imaging features currently known for differentiating this tumor from H3 G34–mutant diffuse hemispheric glioma.

Circumscribed Astrocytic Glioma

These heterogeneous tumors are divided into six tumor families in the 2021 edition of the CNS WHO classification, including pilocytic astrocytoma, high-grade astrocytoma with piloid features, pleomorphic xanthoastrocytoma, subependymal giant cell astrocytoma, choroid glioma, and *MNI*-altered astroblastoma (6).

Pilocytic Astrocytoma

Fusion of *KIAA1549::BRAF* is the most frequent molecular alteration in pediatric low-grade gliomas, with one study reporting the occurrence of this fusion event in 30%–40% of these tumors (18). Pilocytic astrocytomas are CNS WHO grade 1 tumors, which lack *IDH* and *TP53*

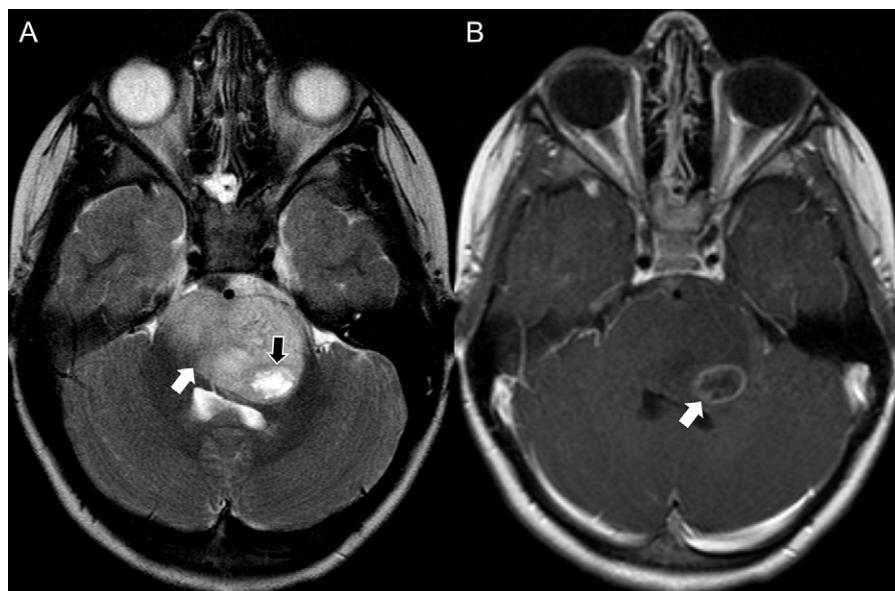


Figure 11: Brain MRI scans in a 6-year-old female patient with diffuse midline high-grade glioma with a K27M amino acid substitution in the histone H3.3 protein. **(A)** Axial T2-weighted image shows a large expansile hyperintense tumor (white arrow) with eccentric necrosis (black arrow). **(B)** Axial contrast-enhanced T1-weighted image shows eccentric necrosis with surrounding enhancement (arrow).

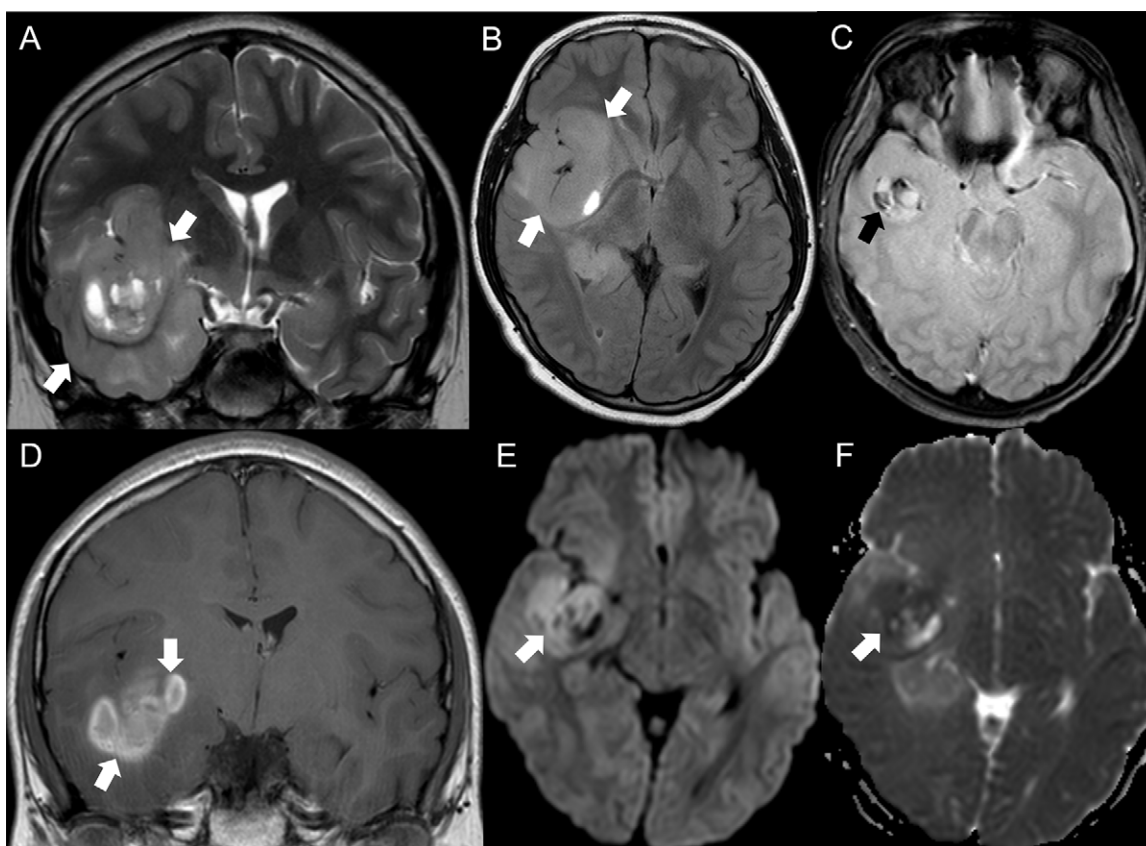


Figure 12: Brain MRI scans in a 13-year-old male patient with right hemispheric diffuse high-grade glioma, isocitrate dehydrogenase–wild type and histone protein H3–wild type, with *MYCN* amplification. **(A)** Coronal T2-weighted image shows a large heterogeneously hyperintense tumor (arrows). **(B)** Axial fluid-attenuated inversion-recovery image shows sharp borders (arrows). **(C)** Axial multiplanar gradient-recalled image shows internal hemorrhage (arrow). **(D)** Coronal contrast-enhanced T1-weighted image shows vivid contrast enhancement (arrows). **(E, F)** Axial diffusion-weighted image **(E)** and apparent diffusion coefficient map **(F)** show partial diffusion restriction of the solid tumor component (arrow).

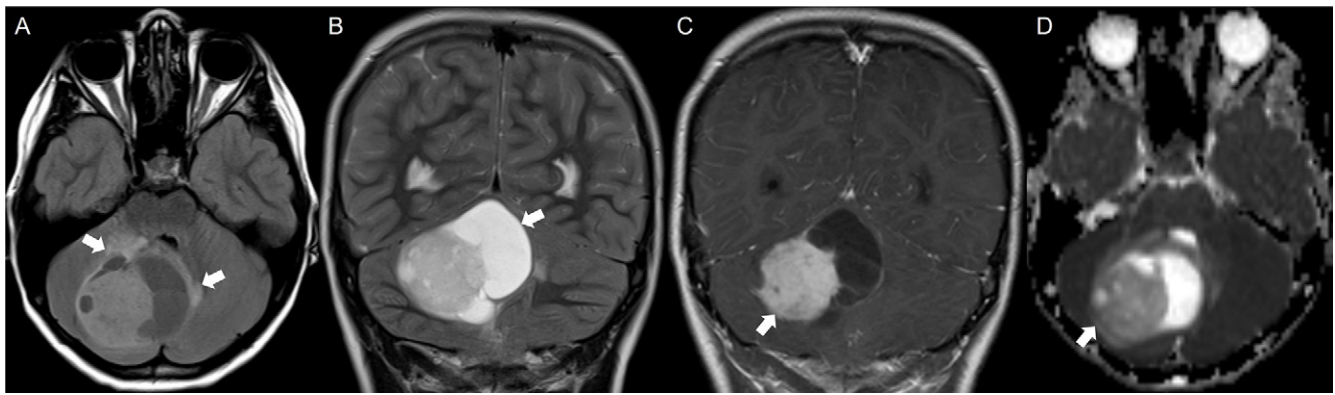


Figure 13: Brain MRI scans in a 9-year-old male patient with cerebellar pilocytic astrocytoma with a *KIAA1549::BRAF* fusion gene. **(A)** Axial fluid-attenuated inversion-recovery image shows a well-circumscribed tumor with mild peripheral edema (arrows). **(B)** Coronal T2-weighted image shows a peripheral cystic component (arrow). **(C)** Coronal contrast-enhanced T1-weighted image shows contrast enhancement of the solid component (arrow). **(D)** Axial apparent diffusion coefficient map shows higher values than gray matter (arrow).

mutations. While 70%–80% of these tumors harbor the MAPK pathway genetic alteration *KIAA1549::BRAF* fusion (20), AYA patients are more likely to have non-*KIAA1549::BRAF* fusion pilocytic astrocytomas (43). These tumors frequently arise from midline structures, including the cerebellum and optic pathway, and are less frequently encountered in the brainstem, cerebral hemispheres, and spinal cord.

Pilocytic astrocytomas typically have a large cystic and smaller contrast-enhancing solid component (mural nodule) on MRI scans (Fig 13A–13C). The cyst wall enhances in approximately half of pilocytic astrocytomas. Calcification is less common and tumor hemorrhage is rare (44,45). The differential diagnoses in the AYA age group mainly include medulloblastoma and ependymoma. Apparent diffusion coefficient values are typically higher than that of gray matter in pilocytic astrocytomas (Fig 13D), while they are lower in medulloblastomas and ependymomas (46).

High-grade Astrocytoma with Piloid Features

In high-grade astrocytomas with piloid features, alterations of the MAPK pathway are often combined with *CDKN2A/B* homozygous deletion and/or *ATRX* mutations and likely represent transformation of long-standing low-grade gliomas or pilocytic astrocytomas. In contrast to pilocytic astrocytomas, the most frequent MAPK pathway alteration detected is *NF1* alteration (31%). High-grade astrocytomas with piloid features most commonly arise in the cerebellum (74%) and are less commonly seen in the supratentorial brain (17%) and spinal cord (7%). Reinhardt et al (47) reported a median patient age of 41.5 years in a study of 83 patients with this high-grade astrocytoma type.

Findings in a series of MRI studies in six patients found that these tumors had a sharp or diffusely infiltrating margin, T1-weighted hypointensity to isointensity, and T2-weighted hyperintense signal. Of the five patients who received a gadolinium-based contrast agent, rim enhancement was seen with a lack of central enhancement in three tumors, while two tumors showed patchy tumor enhancement. No restricted diffusion was noted (48). Based on the limited information available, both high-grade and low-grade glioma need to be considered in the differential diagnosis. In the presence of diffusely infiltrating

tumor margins, the lack of diffusion restriction can help differentiate this tumor type from high-grade gliomas.

Pleomorphic Xanthoastrocytoma

Pleomorphic xanthoastrocytomas are designated CNS WHO grade 2 or 3, depending on histology. Approximately 80%–90% of these tumors harbor a *BRAF* p.V600E mutation and most will also have co-occurring homozygous *CDKN2A/B* deletion (21). Typically, pleomorphic xanthoastrocytomas are located peripherally in the supratentorial brain, with up to 50% observed in the temporal lobe (49). In a study of 50 patients, the mean age at presentation was reported to be 26 years (50).

At MRI, pleomorphic xanthoastrocytoma appears as a solid contrast-enhancing nodule (Fig 14C, 14D). In higher-grade pleomorphic xanthoastrocytomas, contrast enhancement was reported to be more heterogeneous and peritumoral edema was larger. Most pleomorphic xanthoastrocytomas have a peripheral cystic component (Fig 14A, 14B) and apparent diffusion coefficient values are reported to be lower than that found in supratentorial pilocytic astrocytomas (51). A “dural tail sign” is commonly seen, likely due to dural involvement (52). While some pleomorphic xanthoastrocytomas may resemble meningiomas, their cystic component, solid nodule, and T2-weighted signal can typically be used to differentiate them from meningiomas (Fig 14A, 14B) (53). Another characteristic imaging feature of these slow-growing tumors is superficial remodeling (scalloping) of the adjacent skull (Fig 14B) (49). Notably, in a study of 50 adult patients (age range, 18–67 years), almost 50% of pleomorphic xanthoastrocytomas recurred or demonstrated progression to CNS WHO grade 3 (50). The differential diagnoses in AYA patients also include gangliogliomas and dysembryoplastic neuroepithelial tumors. The former can appear very similar but do not demonstrate a dural tail sign. The latter typically have a “bubbly appearance” and less vivid contrast enhancement.

Chordoid Glioma

These rare and slow-growing CNS WHO grade 2 tumors usually arise in the anterior part of the third ventricle with possible extension to the suprasellar region and lateral ventricles (54).

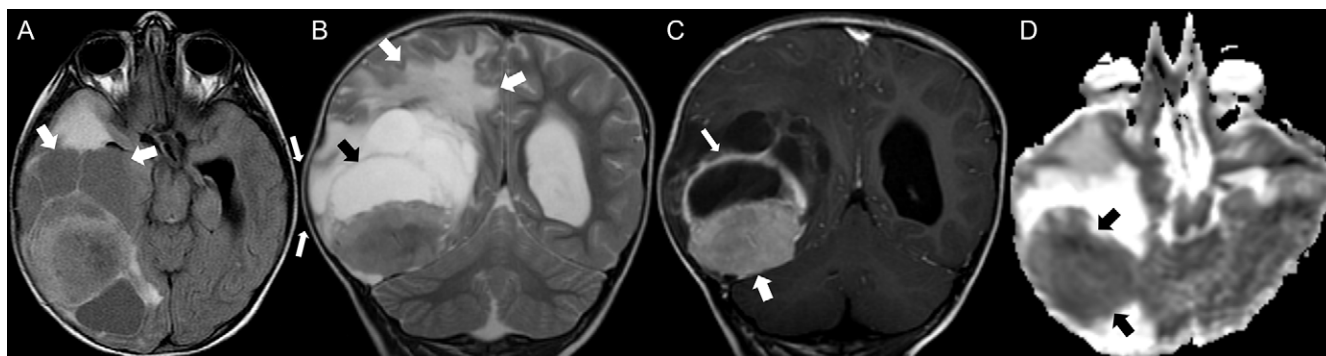


Figure 14: Brain MRI scans in a 5-year-old female patient with large right hemispheric pleomorphic xanthoastrocytoma with a *BRAF* p.V600E mutant protein and *CDKN2A* deletion. **(A)** Axial fluid-attenuated inversion-recovery image shows a large tumor with heterogeneous signal characteristics due to solid and cystic components (arrows). **(B)** Coronal T2-weighted image shows peripheral cystic component (black arrow), extensive perilesional edema (white arrows), and scalloping of the adjacent calvarium (arrows between **A** and **B**). **(C)** Coronal contrast-enhanced T1-weighted image shows contrast enhancement of the cyst wall (thin arrow) and the solid nodule (thick arrow). **(D)** Axial apparent diffusion coefficient map shows low apparent diffusion coefficient values, suggestive of a high cell density (arrows).

Mutations in the *PRKCA* gene have been reported in 80%–90% of chordoid gliomas, leading to enhanced proliferation of astrocytes and tanycytes (20,55). Chordoid gliomas mostly occur in adults (mean age, 46 years) with a female predominance, but they can occur in the AYA age range (55).

At MRI, chordoid gliomas usually appear as well-circumscribed ovoid lesions located in the anterior aspect of the third ventricle. They are isointense on T1-weighted images and hyperintense on T2-weighted images. These tumors demonstrate avid contrast enhancement and peripheral edema, and cysts or calcifications may be present (54,56). The list of differential diagnoses includes intraventricular meningioma, pilocytic astrocytoma, craniopharyngioma, and subependymal giant cell astrocytoma. Pilocytic astrocytomas arise from the optic pathway and may extend toward the hypothalamus and anterior third ventricle, while chordoid gliomas are centered in the anterior third ventricle. Craniopharyngiomas can be differentiated by their intrasellar tumor component and typical signal characteristics. Subependymal giant cell astrocytoma should be considered in the presence of other imaging findings of tuberous sclerosis complex.

Astroblastoma, *MNI*-altered

Astroblastomas with *MNI* alterations are well-circumscribed tumors predominantly encountered in the cerebral hemispheres, most frequently in the frontal and parietal lobes, with few tumors reported to occur in the posterior fossa and spine (19,57). Diagnosis is dependent on the presence of an alteration of protein-encoding proto-oncogene *MNI* on chromosome 22 in combination with the histologic hallmark of astroblastic pseudorosette (58,59). These tumors have a strong female predominance, and the median age at diagnosis was 13.5 years (age range, 2–40 years) in a study of 73 patients (57).

At MRI, these tumors have been reported to be well demarcated with solid and cystic components, heterogeneous contrast enhancement, and mild or no perilesional edema (30,57). On susceptibility-weighted images, abundant susceptibility artifacts have been observed due to hemorrhage and/or calcification (30). Furthermore, restricted diffusion was noted in the solid portions of the tumor (30). Notably, these astroblastomas with *MNI* alterations

frequently recur, with a recent meta-analysis observing up to 62% recurrence across 12 studies (57). In patients with these tumors, 10-year overall survival was reported to be 55% (57). Main differential diagnoses are hemispheric high-grade gliomas, atypical teratoid rhabdoid tumors, and supratentorial ependymomas. While the presence of restricted diffusion is suggestive of a hemispheric high-grade glioma, there is relatively little perilesional edema in astroblastomas with *MNI* alterations. Supratentorial atypical teratoid rhabdoid tumors may have similar MRI features but typically manifest in very young children. Supratentorial ependymoma can be difficult to exclude as a differential diagnosis.

Glioneuronal Tumor

Glioneuronal tumors are a heterogeneous group of rare tumors representing 0.4%–2% of all CNS tumors (60,61). In North America, the annual incidence rate of glioneuronal tumors in the AYA population ranges from 0.4 to 0.49 per 100 000 (1,62). These tumors have a predilection for the temporal lobe and often occur with seizures, accounting for the vast majority of long-term epilepsy-associated tumors (63). Herein, we focus on the more commonly encountered dysembryoplastic neuroepithelial tumors, gangliogliomas, and multinodular and vacuolating neuronal tumors.

Dysembryoplastic Neuroepithelial Tumor

Dysembryoplastic neuroepithelial tumors are slow-growing CNS WHO grade 1 tumors typically located in cortical gray matter, with the most common locations being in the temporal lobe followed by the frontal lobe (64). Duplication of the tyrosine kinase domain of *FGFR1* and *FGFR1* single-nucleotide variants occur in 20%–30% of patients. Less frequent molecular alterations include *FGFR1-TACC1* fusions, which have been reported in 10%–15% of patients (20).

On MRI scans, dysembryoplastic neuroepithelial tumors are often encountered as T1-weighted hypointense, T2/FLAIR hyperintense (Fig 15A, 15B), and multicystic lesions involving cortex with a “bubbly appearance.” On FLAIR images, the cystic component is partially suppressed, which results in a hypointense appearance, while the tumor rim appears hyperintense (65).

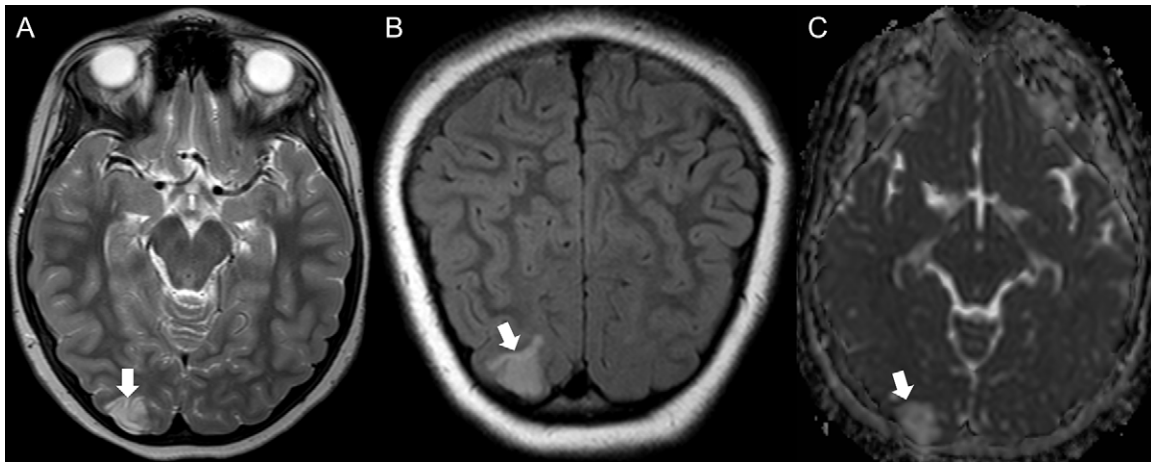


Figure 15: Brain MRI scans in an 11-year-old female patient with right occipital dysembryoplastic neuroepithelial tumor and duplication of the *FGFR1* tyrosine kinase domain. **(A)** Axial T2-weighted image shows a cortical and subcortical hyperintense lesion (arrow). **(B)** Coronal fluid-attenuated inversion-recovery image shows that the hyperintense lesion (arrow) is well delineated. **(C)** Axial apparent diffusion coefficient map shows facilitated diffusivity (arrow).

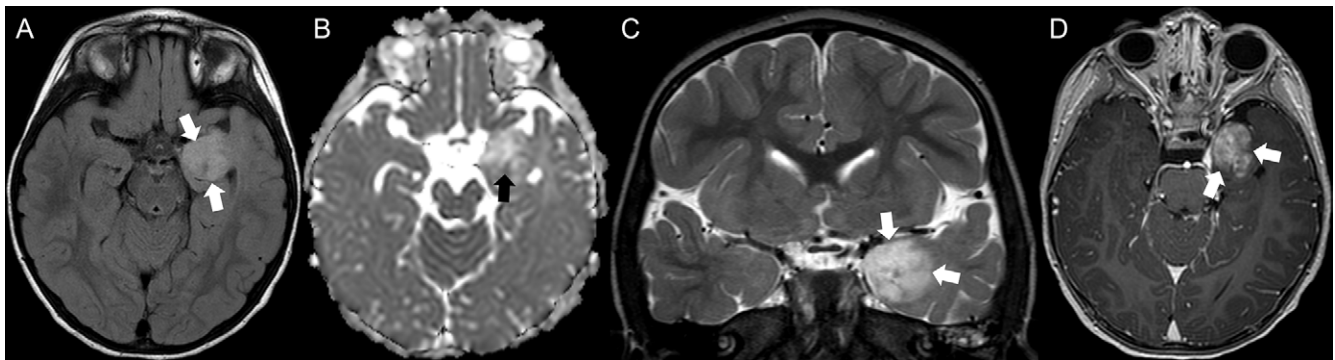


Figure 16: Brain MRI scans in a 2-year-old male patient with left mesial temporal lobe ganglioglioma with a *BRAF* p.V600E mutant protein. **(A)** Axial fluid-attenuated inversion-recovery image shows a hyperintense expansile tumor (arrows). **(B)** Axial apparent diffusion coefficient map shows facilitated diffusivity (arrow). **(C)** Coronal T2-weighted image shows involvement of cortical gray matter and subcortical white matter (arrows). **(D)** Axial contrast-enhanced T1-weighted image shows heterogeneous contrast enhancement (arrows).

There is no restricted diffusion (Fig 15C). Faint nodular or patchy contrast enhancement is reported in 20%–40% of patients. Intratumoral calcifications are seen in one-third of patients (66,67). Several tumor entities may appear similar to dysembryoplastic neuroepithelial tumors, including multinodular and vacuolating neuronal tumors, gangliogliomas, and IDH-mutated low-grade astrocytomas. Multinodular and vacuolating neuronal tumors do not involve the cortex and remain hyperintense, without signal suppression, on FLAIR images. Gangliogliomas commonly demonstrate contrast enhancement and do not have a “bubbly appearance.” Low-grade astrocytomas are usually confined to white matter, with mass effect on the overlying cortex.

Ganglioglioma

The majority of gangliogliomas are CNS WHO grade 1 and typically diagnosed from 10 to 30 years of age (61). Approximately 40%–50% of gangliogliomas exhibit *BRAF* p.V600E mutation and another 10%–15% exhibit *KIAA1549::BRAF* fusion (20). Gangliogliomas are most frequently found in the temporal lobes but can occur anywhere in the CNS.

While these tumors have variable imaging characteristics, the classic appearance at MRI is that of a cystic tumor with an avidly enhancing mural nodule. Less commonly, they are seen as a T2-weighted hyperintense (Fig 16A–16C), solid, and well-circumscribed mass lesion with a variable degree of contrast enhancement (Fig 16D). Calcification is frequent, perilesional edema is uncommon, and restricted diffusion is usually absent (Fig 16B). There may be remodeling of the adjacent calvarium with scalloping. MRI perfusion may demonstrate greater relative cerebral blood volume than other low-grade tumors (61). The differential diagnoses include dysembryoplastic neuroepithelial tumors and pleomorphic xanthoastrocytomas.

Multinodular and Vacuolating Neuronal Tumor

Multinodular and vacuolating neuronal tumors are now recognized as a distinct entity in the 2021 CNS WHO classification of brain tumors (6). They are seizure-associated low-grade tumors predominantly seen in subcortical white matter, but cortical involvement is possible (68). The identification of genetic abnormalities (*MAP2K1* alteration in 50%–60% of patients, *BRAF* p.V600E in 5%–10% of patients) (20) suggests a

Table 3: Molecular Markers and MRI Features of Ependymoma Included in the WHO Classification of Tumors of the Central Nervous System, Fifth Edition

Compartment and Histology	WHO Grade	Molecular Characteristic	Age Group	Imaging Feature
Supratentorial				
Subependymoma	1		Adults	Most frequently, fourth ventricle, then lateral ventricles, T2-weighted hyperintense with more heterogeneous appearance in larger lesions, possible calcifications; usually, perilesional edema and nonenhancing
Ependymoma	2/3	<i>ZFTA</i> fusion	All age groups	Frontal and parietal lobe, cystic, solid component with diffusion restriction and enhancement, peritumoral edema and internal hemorrhage
Ependymoma	2/3	<i>YAPI</i> fusion	Infants, children	Large at presentation with prominent cystic components and solid component with heterogeneous enhancement and variable perilesional edema
Posterior fossa				
Subependymoma	1		Adults	Same as above
Ependymoma	2/3	PFA (H3 K27 trimethylation loss, <i>EZH2</i> positive)	Infants, children	Likely to arise from roof or lateral portions of fourth ventricle, calcification more common than in PFB
Ependymoma	2/3	PFB (H3 K27 trimethylation retained, <i>EZH2</i> not expressed)	Adolescents, adults	Frequently arises from fourth ventricular floor, cyst formation, greater enhancement than PFA
Spinal				
Myxopapillary ependymoma	2		Adolescents, adults	Well defined at conus medullaris and cauda equina, "sausage-shaped," contrast enhancing, extending more than one vertebral level
Ependymoma	2/3	<i>MYCN</i> -amplified	Adults	Large at presentation with infiltration of the cord over several vertebral segments, commonly leptomeningeal disease at presentation
Ependymoma	2/3	No <i>MYCN</i> amplification	Commonly adults	Heterogeneous appearance with enhancement of solid portions, cystic and necrotic changes, hemorrhage

Note.—*EZH2* = EZH inhibitory protein, *MYCN* = N-Myc proto-oncogene protein, PFA = posterior fossa ependymoma type A, PFB = posterior fossa ependymoma type B, WHO = World Health Organization, *YAPI* = yes1-associated transcriptional regulator, *ZFTA* = zinc finger translocation-associated.

neoplastic rather than a malformative origin (60). While multinodular and vacuolating neuronal tumors most commonly occur in adults older than 30 years and may be seen as an incidental radiologic finding, they are observed in the AYA age range (60,61,69).

These tumors have a characteristic appearance on MRI scans. Lesions are juxtacortical and subcortical and consist of multiple small well-defined nodules that appear hyperintense with T2-weighted and FLAIR sequences. Nodules appear without mass effect, surrounding edema, calcification, or diffusion restriction. Contrast enhancement is also usually absent (60,61,69). The main differential diagnosis is dysembryoplastic neuroepithelial tumors in which the cystic components suppress to hypointense signal on FLAIR images.

Ependymoma

According to the fifth edition of the CNS WHO classification, ependymomas are grouped based on anatomic location, including the supratentorial, posterior fossa, and spinal compartments. Overall, there are 10 subgroups according to a combination of histopathologic, anatomic, and molecular features (Table 3).

CNS WHO grades 2 and 3 continue to be defined according to histologic features in ependymomas (6).

Supratentorial Ependymoma

There are two molecular groups of supratentorial ependymomas harboring either *ZFTA* gene fusions or *YAPI* gene fusions. In the 2021 classification of brain tumors, what was once termed the *RELA* fusion-positive ependymoma group is now referred to as *ZFTA* fusion-positive, as *ZFTA* gene fusion was found to be slightly more prevalent in this tumor type than *RELA* gene fusion (6). In the AYA population, the *ZFTA* fusion-positive subgroup accounts for the majority of supratentorial ependymomas. Gene fusions with *YAPI* are largely restricted to infants and young children (70).

Supratentorial ependymomas have a heterogeneous appearance on MRI scans. In an analysis of 47 *RELA*-fused supratentorial ependymomas (mean age, 7.9 years \pm 5.2 [SD]), most were located in the frontal or parietal lobes (Fig 17A), with only few tumors arising solely in intraventricular or extra-axial regions (71). Tumors were mostly cystic, with possible central necrosis (Fig 17A), diffusion restriction (Fig 17B), and contrast enhancement

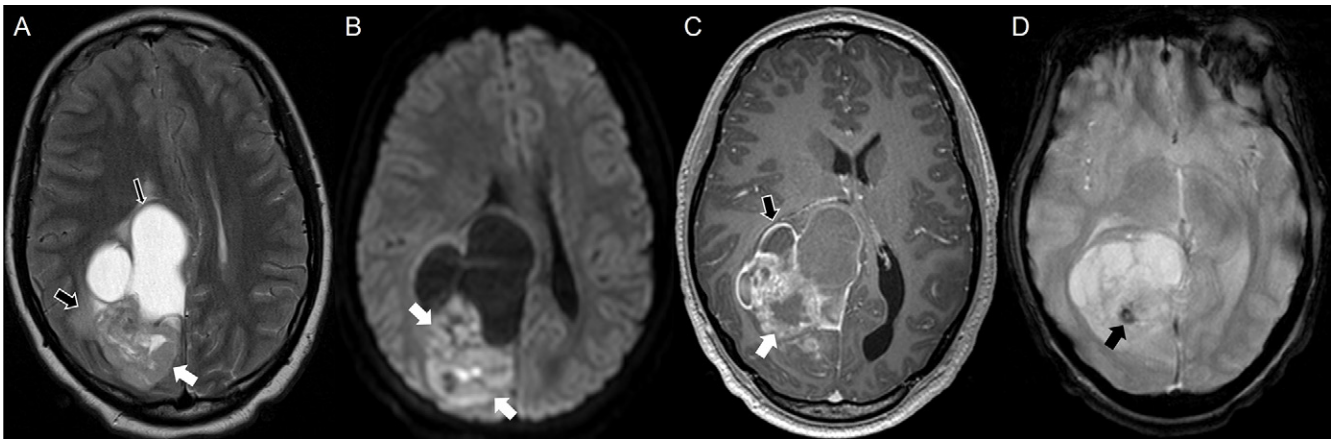


Figure 17: Brain MRI scans in a 14-year-old female patient with a supratentorial ependymoma that is *ZFTA*-fusion positive. **(A)** Axial T2-weighted image shows a solid (white arrow) and cystic (thin black arrow) tumor centered in the right parietal lobe with mild perilesional edema (thick black arrow). **(B)** Axial diffusion-weighted image shows diffusion restriction of the solid component (arrows). **(C)** Axial contrast-enhanced T1-weighted image shows heterogeneous contrast enhancement of the solid component (white arrow) and the cyst wall (black arrow). **(D)** Axial T2*-weighted image demonstrates a small intratumoral hemorrhage (arrow).

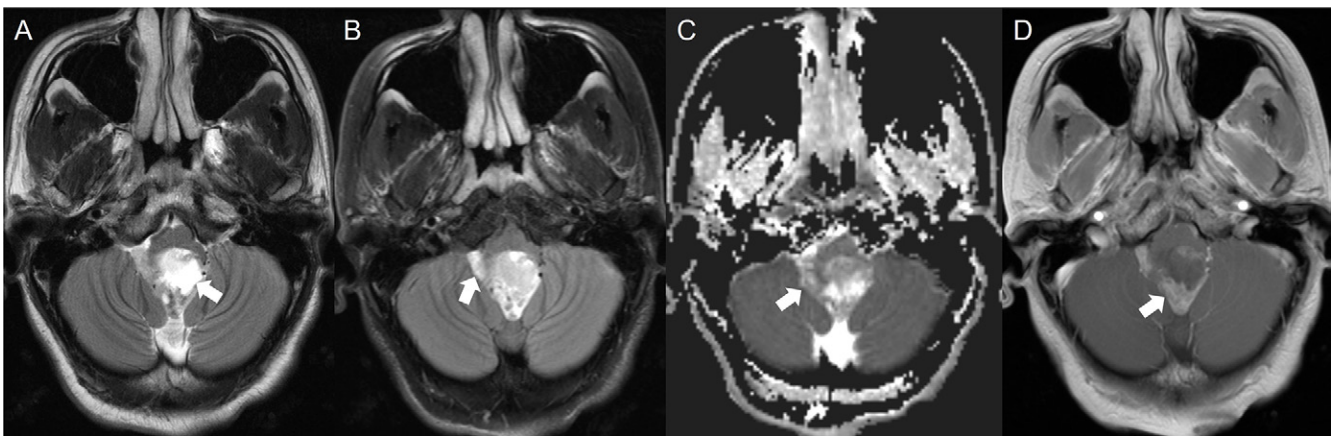


Figure 18: Brain MRI scans in a 29-year-old male patient with posterior fossa type B ependymoma with retained histone H3 K27 trimethylation and nonexpression of *EZH1P*. **(A)** Axial T2-weighted image shows hyperintense tumor in the fourth ventricular floor and right, more than left, foramina of Luschka (arrow). **(B)** Axial fluid-attenuated inversion-recovery image shows the hyperintense tumor with extension through the left foramen of Luschka (arrow). **(C)** Axial apparent diffusion coefficient map shows lower apparent diffusion coefficient values for the solid tumor component (arrow). **(D)** Axial contrast-enhanced T1-weighted image shows partial enhancement of the solid portions (arrow).

of their solid component (Fig 17C). Perilesional edema was a common finding (Fig 17A). Signs of intratumoral hemorrhage (Fig 17D) were found in 27 of 45 patients (60%) (71). Supratentorial ependymomas that are *YAPI* fusion-positive are typically large at presentation, with prominent cystic components and a solid component with heterogeneous enhancement and variable perilesional edema (72). Supratentorial ependymomas may be difficult to distinguish from their imaging differential diagnoses, including glioblastoma, oligodendroglioma, metastasis, and astroblastoma. If small, oligodendrogliomas may be differentiated by their cortical location. Metastases more commonly occur at the gray-white matter interface and often demonstrate larger edema than expected for their size.

Posterior Fossa Ependymoma

Most posterior fossa type A ependymomas occur in infants and younger children. In adolescence, 50% of posterior fossa ependymomas are type B, while in patients older than 18 years, more

than 90% are type B (5,73). Type A tumors exhibit overexpression of *EZH1P* and associated loss of H3 K27 trimethylation, while type B tumors show no *EZH1P* expression and retain H3 K27 trimethylation (74,75). It should be noted that lack of *EZH1P* expression is not specific to posterior fossa ependymoma type B and does not distinguish this type of ependymoma from subependymoma.

Type A ependymomas are more likely to arise from the roof or lateral portions of the fourth ventricle, whereas type B ependymomas more frequently arise from the fourth ventricular floor (76,77). Posterior fossa ependymomas often extend through the fourth ventricular outlets (Fig 18). In an imaging study with 16 patients, calcification was more commonly seen in type A ependymomas, whereas cyst formation was only seen in type B. Furthermore, the contrast-enhancing tumor component (Fig 18D) was reported as larger in posterior fossa ependymoma type B (78). Long-term follow-up is important in AYA patients with type B as late relapses are not uncommon

Table 4: Molecular Markers and MRI Features of Medulloblastoma

Subgroup	Overall Frequency	Age Group	Anatomic Location	Imaging Feature
WNT-activated	10%	Children, adolescents, adults	Foramen of Luschka, fourth ventricle; more commonly, cisterna magna, cerebellopontine angle cistern	Mild to avid enhancement, necrosis and hemorrhage are common
SHH-activated (<i>TP53</i> wild type and <i>TP53</i> -mutated)	30%	Infants and adults (<i>TP53</i> wild type), children (<i>TP53</i> -mutated)	Cerebellar hemispheres	Solid enhancement more common than other groups, hemorrhage
Non-WNT, non-SHH group 3 and group 4	25% and 35%, respectively	Mostly children	Midline and fourth ventricle	Ill-defined margins with leptomeningeal enhancement in infants, minimal or no enhancement in group 4, hemorrhage in group 4, hypercellularity with diffusion restriction

Note.—Information provided in the table is based on references 80, 81, and 84. SHH = sonic hedgehog, WNT = wingless type.

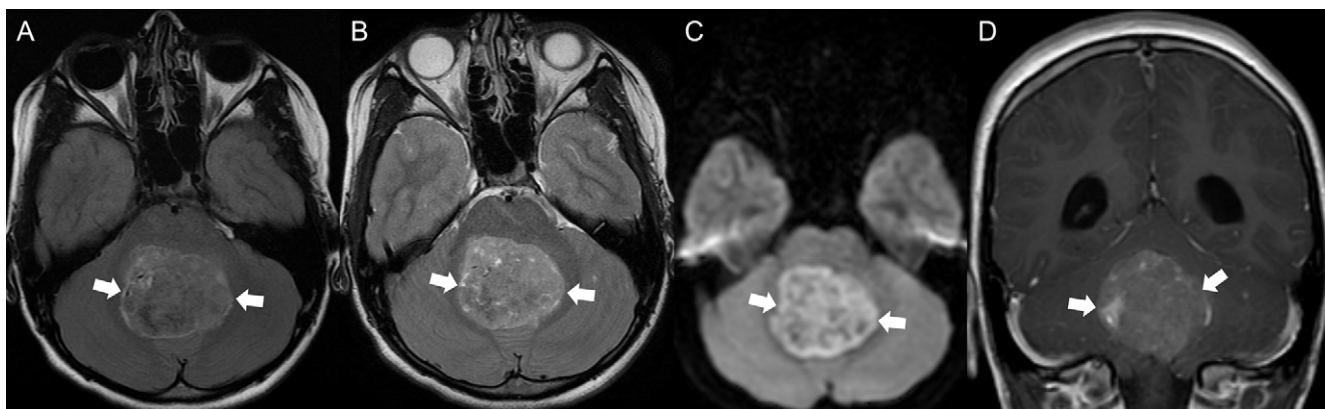


Figure 19: Brain MRI scans in an 11-year-old male patient with wingless-type-activated medulloblastoma in the fourth ventricle. **(A)** Axial fluid-attenuated inversion-recovery image shows a large partially hypointense-to-isointense tumor (arrows). **(B)** Axial T2-weighted image shows that the tumor is well delineated (arrows) and without peripheral edema. **(C)** Axial diffusion-weighted image shows diffusion restriction (arrows). **(D)** Coronal contrast-enhanced T1-weighted image shows moderate enhancement (arrows).

(79). Main differential diagnoses are medulloblastomas and pilocytic astrocytomas. In a study of 148 children with posterior fossa tumors, ependymomas were differentiated from pilocytic astrocytomas and medulloblastomas by a fourth ventricular location, a high or intermediate apparent diffusion coefficient compared with gray matter, and the presence of cystic, hemorrhagic, or calcific areas (46).

Medulloblastoma

Medulloblastoma is the most common malignant embryonal tumor in the AYA population. The prevalence of medulloblastoma subgroups and prognostic markers differ between children and adults, with different treatment strategies and outcome predictors (Table 4) (5). The 2021 CNS WHO tumor classification retains the four subgroups from the 2016 classification, including wingless-type (WNT)-activated, sonic hedgehog (SHH)-activated (which can be either *TP53*-wild type or *TP53*-mutant),

and non-WNT/non-SHH group 3 and group 4. Group 3 and group 4 tumors comprise multiple molecular subgroups that are identified by DNA methylation profiling (6,16,80,81). Group 3 tumors are very rare in AYAs and adults (<2%). For ages 10–18 years, the predominant medulloblastoma types are WNT-activated and non-WNT/non-SHH group 4. In the AYA and adult populations, the majority of medulloblastomas are SHH-activated (60%), followed by non-WNT/non-SHH group 4 and WNT-activated tumors (82).

Medulloblastomas with WNT activation commonly involve the foramina of Luschka and fourth ventricle, and less commonly involve the cisterna magna and cerebellopontine angle cistern (83). On MRI scans, mild to avid contrast enhancement is observed (Fig 19), and necrosis and hemorrhage are common (83–85). Medulloblastomas with SHH activation mainly arise in the cerebellar hemispheres (Fig 20) (86). Group 3 and group 4 medulloblastomas more frequently arise from

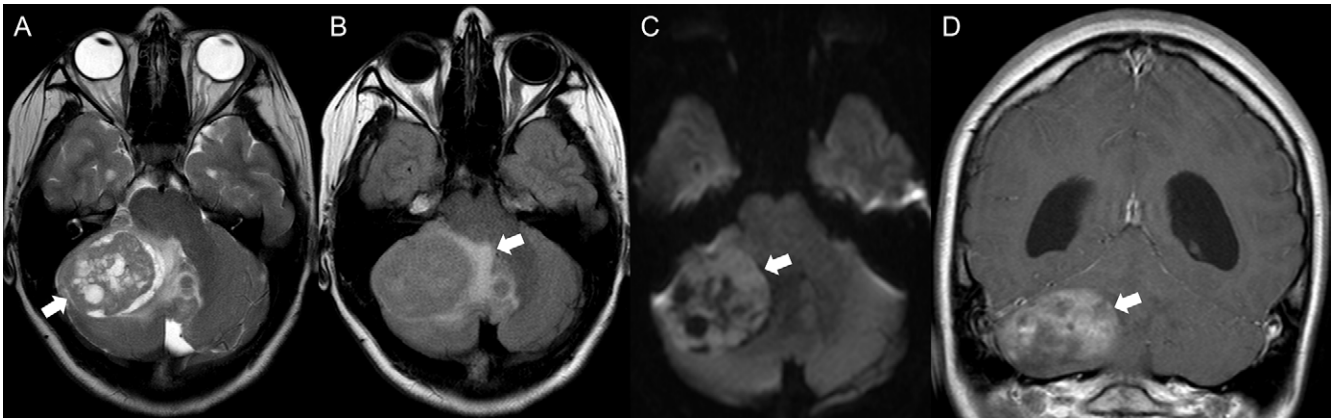


Figure 20: Brain MRI scans in a 14-year-old female patient with sonic hedgehog–activated medulloblastoma in the right cerebellar hemisphere. **(A)** Axial T2-weighted image shows a solid and cystic tumor (arrow). **(B)** Axial fluid-attenuated inversion-recovery image shows perilesional edema (arrow). **(C)** Axial diffusion-weighted image shows restricted diffusion of the solid tumor component (arrow). **(D)** Coronal contrast-enhanced T1-weighted image shows heterogeneous enhancement (arrow).



Figure 21: Brain MRI scans in a 3-year-old male patient with a non–wingless-type non–sonic hedgehog medulloblastoma group 3 tumor arising from the vermis. **(A)** Axial T2-weighted image shows an ill-defined tumor in the vermis (arrows). **(B)** Axial fluid-attenuated inversion-recovery image shows perilesional edema (thick white arrow) and a hyperintense left cerebellar metastasis (thin white arrow). **(C)** Axial apparent diffusion coefficient map shows low apparent diffusion coefficient values, which indicate high cell density (arrow). **(D)** Coronal contrast-enhanced T1-weighted image shows leptomeningeal metastatic spread (thin white arrows) and avid enhancement of the tumor (thick white arrow) with left lateral cerebellar metastasis (circle).

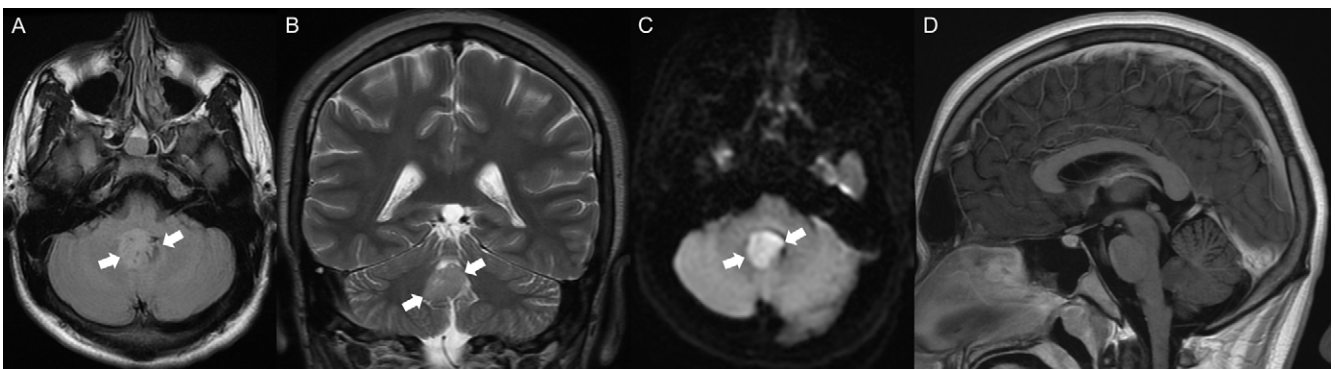


Figure 22: Brain MRI scans in a 17-year-old male patient with a non–wingless-type non–sonic hedgehog medulloblastoma group 4 tumor arising from the vermis. **(A)** Axial fluid-attenuated inversion-recovery image shows a mildly hyperintense solid tumor (arrows). **(B)** Coronal T2-weighted image shows that the tumor is well delineated (arrows) and without perilesional edema. **(C)** Axial diffusion-weighted image shows diffusion restriction (arrows). **(D)** Coronal contrast-enhanced T1-weighted image shows absent enhancement.

the vermis (Figs 21, 22). Group 4 medulloblastomas exhibit fainter enhancement than group 3 medulloblastomas (Figs 21D, 22D) (83,87,88). In adult SHH-activated medulloblastoma, most recurrences are located in the local tumor bed and

outside the neural axis, whereas group 4 medulloblastomas tend to recur with leptomeningeal metastasis and not in the local tumor bed (89). Main differential diagnoses are ependymomas and pilocytic astrocytomas. In a study of 148 children

with posterior fossa tumors, SHH-activated medulloblastomas were differentiated from pilocytic astrocytoma and ependymoma by their location in the cerebellar hemispheres or fourth ventricle, a lower apparent diffusion coefficient compared with gray matter, and an extra-axial appearance or the presence of multiple enhancing nodules (46).

Conclusion

Adolescents and young adults (AYAs) are recognized as an overlooked population that needs multidisciplinary and specialized care across the transition phase from pediatric to adult specialization. Radiologists interpreting neuroimaging studies for AYA patients must be familiar with tumor-specific imaging findings across pediatric and adult brain tumors to facilitate optimal patient care. Understanding of the biology of brain tumors is rapidly advancing, which is reflected in changes to the World Health Organization classification of these tumors. As radiologists, we need to become familiar with new tumor types, adopt updated nomenclatures, and drop outdated tumor designations when providing imaging care for AYA patients with brain tumors.

Disclosures of conflicts of interest: M.W.W. No relevant relationships. P.J.M. No relevant relationships. J.B. No relevant relationships. L.N. No relevant relationships. M.J.L.F. No relevant relationships. P.D. No relevant relationships. S.L. No relevant relationships. U.T. No relevant relationships. V.R. No relevant relationships. C.H. No relevant relationships. B.B.E.W. *Radiology* editorial board; grants or contracts from Bayer Healthcare; member of Board of Directors, American Society of Pediatric Neuroradiology; stock or stock options in Munich Medical International; spouse is an employee for Siemens Healthineers.

References

- Ostrom QT, Price M, Neff C, et al. CBTRUS Statistical Report: Primary Brain and Other Central Nervous System Tumors Diagnosed in the United States in 2015-2019. *Neuro Oncol* 2022;24(Suppl 5):v1-v95.
- Yeo KK, Burgers DE, Brodigan K, et al. Adolescent and young adult neuro-oncology: a comprehensive review. *Neurooncol Pract* 2021;8(3):236-246.
- Zumel-Marne A, Kundi M, Castaño-Vinyals G, et al. Clinical presentation of young people (10-24 years old) with brain tumors: results from the international MOBI-Kids study. *J Neurooncol* 2020;147(2):427-440.
- Papageorgiou GI, Razis ED. CNS Tumors in Adolescents and Young Adults: The Need for a Holistic Specialized Approach. *JCO Oncol Pract* 2020;16(4):155-162.
- Lim-Fat MJ, Macdonald M, Lapointe S, et al. Molecular testing for adolescent and young adult central nervous system tumors: A Canadian guideline. *Front Oncol* 2022;12:960509.
- Louis DN, Perry A, Wesseling P, et al. The 2021 WHO Classification of Tumors of the Central Nervous System: a summary. *Neuro Oncol* 2021;23(8):1231-1251.
- Patel SH, Poisson LM, Brat DJ, et al. T2-FLAIR Mismatch, an Imaging Biomarker for IDH and 1p/19q Status in Lower-grade Gliomas: A TCGA/TCIA Project. *Clin Cancer Res* 2017;23(20):6078-6085.
- Do YA, Cho SJ, Choi BS, et al. Predictive accuracy of T2-FLAIR mismatch sign for the IDH-mutant, 1p/19q noncodeleted low-grade glioma: An updated systematic review and meta-analysis. *Neurooncol Adv* 2022;4(1):vdac010.
- Johnson DR, Kaufmann TJ, Patel SH, Chi AS, Snuderl M, Jain R. There is an exception to every rule-T2-FLAIR mismatch sign in gliomas. *Neuroradiology* 2019;61(2):225-227.
- Feraco P, Franciosi R, Picori L, Scalorbi F, Gagliardo C. Conventional MRI-Derived Biomarkers of Adult-Type Diffuse Glioma Molecular Subtypes: A Comprehensive Review. *Biomedicines* 2022;10(10):2490.
- Johnson DR, Giannini C, Vaubel RA, et al. A Radiologist's Guide to the 2021 WHO Central Nervous System Tumor Classification: Part I-Key Concepts and the Spectrum of Diffuse Gliomas. *Radiology* 2022;304(3):494-508.
- Smits M. Imaging of oligodendroglioma. *Br J Radiol* 2016;89(1060):20150857.
- Fellah S, Caudal D, De Paula AM, et al. Multimodal MR imaging (diffusion, perfusion, and spectroscopy): is it possible to distinguish oligodendroglial tumor grade and 1p/19q codeletion in the pretherapeutic diagnosis? *AJNR Am J Neuroradiol* 2013;34(7):1326-1333.
- van Lent DI, van Baarsen KM, Snijders TJ, Robe PAJT. Radiological differences between subtypes of WHO 2016 grade II-III gliomas: a systematic review and meta-analysis. *Neurooncol Adv* 2020;2(1):vdaa044.
- Roux A, Tauziède-Espariat A, Zanello M, et al. Imaging growth as a predictor of grade of malignancy and aggressiveness of IDH-mutant and 1p/19q-codeleted oligodendrogliomas in adults. *Neuro Oncol* 2020;22(7):993-1005.
- Louis DN, Perry A, Reifenberger G, et al. The 2016 World Health Organization Classification of Tumors of the Central Nervous System: a summary. *Acta Neuropathol (Berl)* 2016;131(6):803-820.
- Latysheva A, Emblem KE, Brandal P, et al. Dynamic susceptibility contrast and diffusion MR imaging identify oligodendroglioma as defined by the 2016 WHO classification for brain tumors: histogram analysis approach. *Neuroradiology* 2019;61(5):545-555.
- Ryall S, Zapotocky M, Fukuoka K, et al. Integrated Molecular and Clinical Analysis of 1,000 Pediatric Low-Grade Gliomas. *Cancer Cell* 2020;37(4):569-583.e5.
- McNamara C, Mankad K, Thust S, et al. 2021 WHO classification of tumours of the central nervous system: a review for the neuroradiologist. *Neuroradiology* 2022;64(10):1919-1950.
- Ryall S, Tabori U, Hawkins C. Pediatric low-grade glioma in the era of molecular diagnostics. *Acta Neuropathol Commun* 2020;8(1):30.
- Chiang J, Harrelld JH, Tinkle CL, et al. A single-center study of the clinicopathologic correlates of gliomas with a MYB or MYBL1 alteration. *Acta Neuropathol (Berl)* 2019;138(6):1091-1092.
- Kalioglu T, Rama B, Cho BB, Lopes BM, Patel SH. Pediatric-type diffuse low-grade glioma with *MYB/MYBL1* alteration: report of 2 cases. *Neuroradiol J* 2023;36(2):232-235.
- Wagner MW, Nobre L, Namdar K, et al. T2-FLAIR Mismatch Sign in Pediatric Low-Grade Glioma. *AJNR Am J Neuroradiol* 2023;44(7):841-845.
- Koral K, Koral KM, Sklar F. Angiocentric glioma in a 4-year-old boy: imaging characteristics and review of the literature. *Clin Imaging* 2012;36(1):61-64.
- Lellouch-Tubiana A, Boddaert N, Bourgeois M, et al. Angiocentric neuroepithelial tumor (ANET): a new epilepsy-related clinicopathological entity with distinctive MRI. *Brain Pathol* 2005;15(4):281-286.
- Bale TA, Rosenblum MK. The 2021 WHO Classification of Tumors of the Central Nervous System: An update on pediatric low-grade gliomas and glioneuronal tumors. *Brain Pathol* 2022;32(4):e13060.
- Huse JT, Snuderl M, Jones DT, et al. Polymorphous low-grade neuroepithelial tumor of the young (PLNTY): an epileptogenic neoplasm with oligodendroglioma-like components, aberrant CD34 expression, and genetic alterations involving the MAP kinase pathway. *Acta Neuropathol (Berl)* 2017;133(3):417-429.
- Fei X, Zhao J, Wei W, et al. Clinical, Radiological, Pathological Features and Seizure Outcome With Surgical Management of Polymorphous Low-Grade Neuroepithelial Tumor of the Young Associated With Epilepsy. *Front Oncol* 2022;12:863373.
- Chen Y, Tian T, Guo X, et al. Polymorphous low-grade neuroepithelial tumor of the young: case report and review focus on the radiological features and genetic alterations. *BMC Neurol* 2020;20(1):123.
- Mhatre R, Sugur HS, Nandeesh BN, Chickabasaviah Y, Saini J, Santosh V. MN1 rearrangement in astroblastoma: study of eight cases and review of literature. *Brain Tumor Pathol* 2019;36(3):112-120.
- Yoshimoto K, Hatae R, Sangatsuda Y, et al. Prevalence and clinicopathological features of H3.3 G34-mutant high-grade gliomas: a retrospective study of 411 consecutive glioma cases in a single institution. *Brain Tumor Pathol* 2017;34(3):103-112.
- Roux A, Pallud J, Saffroy R, et al. High-grade gliomas in adolescents and young adults highlight histomolecular differences from their adult and pediatric counterparts. *Neuro Oncol* 2020;22(8):1190-1202.
- Lim KY, Won JK, Park CK, et al. H3 G34-mutant high-grade glioma. *Brain Tumor Pathol* 2021;38(1):4-13.
- Picart T, Barritault M, Poncet D, et al. Characteristics of diffuse hemispheric gliomas, H3 G34-mutant in adults. *Neurooncol Adv* 2021;3(1):vdab061.
- Puntonet J, Dangouloff-Ros V, Saffroy R, et al. Historadiological correlations in high-grade glioma with the histone 3.3 G34R mutation. *J Neuroradiol* 2018;45(5):316-322.
- Kurokawa R, Baba A, Kurokawa M, et al. Neuroimaging features of diffuse hemispheric glioma, H3 G34-mutant: A case series and systematic review. *J Neuroimaging* 2022;32(1):17-27.
- Sievers P, Sill M, Schrimpf D, et al. A subset of pediatric-type thalamic gliomas share a distinct DNA methylation profile, H3K27me3 loss and frequent alteration of EGFR. *Neuro Oncol* 2021;23(1):34-43.

38. Mondal G, Lee JC, Ravindranathan A, et al. Pediatric bithalamic gliomas have a distinct epigenetic signature and frequent EGFR exon 20 insertions resulting in potential sensitivity to targeted kinase inhibition. *Acta Neuropathol (Berl)* 2020;139(6):1071–1088.
39. Holzapfel J, Kandels D, Schmidt R, et al. Favorable prognosis in pediatric brainstem low-grade glioma: Report from the German SIOP-LGG 2004 cohort. *Int J Cancer* 2020;146(12):3385–3396.
40. Korshunov A, Schrimpf D, Ryzhova M, et al. H3-/IDH-wild type pediatric glioblastoma is comprised of molecularly and prognostically distinct subtypes with associated oncogenic drivers. *Acta Neuropathol (Berl)* 2017;134(3):507–516.
41. Buccoliero AM, Giunti L, Moscardi S, et al. Pediatric High Grade Glioma Classification Criteria and Molecular Features of a Case Series. *Genes (Basel)* 2022;13(4):624.
42. Tauziède-Espariat A, Debily MA, Castel D, et al. The pediatric supratentorial MYCN-amplified high-grade gliomas methylation class presents the same radiological, histopathological and molecular features as their pontine counterparts. *Acta Neuropathol Commun* 2020;8(1):104.
43. Hasselblatt M, Riesmeier B, Lechte B, et al. BRAF-KIAA1549 fusion transcripts are less frequent in pilocytic astrocytomas diagnosed in adults. *Neuropathol Appl Neurobiol* 2011;37(7):803–806.
44. Knight J, De Jesus O. Pilocytic Astrocytoma. In: StatPearls [Internet]. Treasure Island (FL): StatPearls Publishing; 2023 Jan. 2023 Aug 23.
45. Koeller KK, Rushing EJ. From the archives of the AFIP: pilocytic astrocytoma: radiologic-pathologic correlation. *RadioGraphics* 2004;24(6):1693–1708.
46. Alves CAPF, Löbel U, Martin-Saavedra JS, et al. A Diagnostic Algorithm for Posterior Fossa Tumors in Children: A Validation Study. *AJNR Am J Neuroradiol* 2021;42(5):961–968.
47. Reinhardt A, Stichel D, Schrimpf D, et al. Anaplastic astrocytoma with piloid features, a novel molecular class of IDH wildtype glioma with recurrent MAPK pathway, CDKN2A/B and ATRX alterations. *Acta Neuropathol (Berl)* 2018;136(2):273–291.
48. Bender K, Perez E, Chirica M, et al. High-grade astrocytoma with piloid features (HGAP): the Charité experience with a new central nervous system tumor entity. *J Neurooncol* 2021;153(1):109–120.
49. She D, Liu J, Xing Z, Zhang Y, Cao D, Zhang Z. MR Imaging Features of Anaplastic Pleomorphic Xanthoastrocytoma Mimicking High-Grade Astrocytoma. *AJNR Am J Neuroradiol* 2018;39(8):1446–1452.
50. Yan J, Cheng J, Liu F, Liu X. Pleomorphic xanthoastrocytomas of adults: MRI features, molecular markers, and clinical outcomes. *Sci Rep* 2018;8(1):14275.
51. She D, Liu J, Zeng Z, Xing Z, Cao D. Diagnostic accuracy of diffusion weighted imaging for differentiation of supratentorial pilocytic astrocytoma and pleomorphic xanthoastrocytoma. *Neuroradiology* 2018;60(7):725–733.
52. Lim S, Kim JH, Kim SA, Park ES, Ra YS, Kim CJ. Prognostic factors and therapeutic outcomes in 22 patients with pleomorphic xanthoastrocytoma. *J Korean Neurosurg Soc* 2013;53(5):281–287.
53. Sotoudeh H, Yazdi HR. A review on dural tail sign. *World J Radiol* 2010;2(5):188–192.
54. Bongetta D, Riso A, Morbini P, Butti G, Gaetani P. Chordoid glioma: a rare radiologically, histologically, and clinically mystifying lesion. *World J Surg Oncol* 2015;13(1):188.
55. Rosenberg S, Simeonova I, Bielle F, et al. A recurrent point mutation in PRK-CA is a hallmark of chordoid gliomas. *Nat Commun* 2018;9(1):2371.
56. Morais BA, Menendez DF, Medeiros RS, Teixeira MJ, Lepski GA. Chordoid glioma: Case report and review of the literature. *Int J Surg Case Rep* 2015;7C:168–171.
57. Chen W, Soon YY, Pratissey PD, et al. Central nervous system neuroepithelial tumors with MN1-alteration: an individual patient data meta-analysis of 73 cases. *Brain Tumor Pathol* 2020;37(4):145–153.
58. Brat DJ, Hirose Y, Cohen KJ, Feuerstein BG, Burger PC. Astroblastoma: clinicopathologic features and chromosomal abnormalities defined by comparative genomic hybridization. *Brain Pathol* 2000;10(3):342–352.
59. Sturm D, Orr BA, Toprak UH, et al. New Brain Tumor Entities Emerge from Molecular Classification of CNS-PNETs. *Cell* 2016;164(5):1060–1072.
60. Vaz A, Cavalcanti MS, da Silva Junior EB, Ramina R, de Almeida Teixeira BC. Uncommon Glioneuronal Tumors: A Radiologic and Pathologic Synopsis. *AJNR Am J Neuroradiol* 2022;43(8):1080–1089.
61. Abdel Razek AAK, Elsebaie NA, Zamora C, Castillo M. Imaging of Neuronal and Mixed Glioneuronal Tumors. *J Comput Assist Tomogr* 2020;44(3):356–369.
62. Smith T, Yuan Y, Walker E, Davis F. Brain Tumour Registry of Canada (BTRC): Incidence Report 2010-2015. Brain Tumour Registry of Canada (BTRC): A Surveillance Research Collaborative. <https://braintumourregistry.ca/incidence-report/>. Published 2019. Accessed February 23, 2023.
63. Delev D, Daka K, Heynckes S, et al. Long-term epilepsy-associated tumors: transcriptional signatures reflect clinical course. *Sci Rep* 2020;10(1):96.
64. Louis DN, Wiestler OD. WHO Classification of Tumours of the Central Nervous System. International Agency for Research on Cancer, 2016.
65. Parmar HA, Hawkins C, Ozelame R, Chuang S, Rutka J, Blaser S. Fluid-attenuated inversion recovery ring sign as a marker of dysembryoplastic neuroepithelial tumors. *J Comput Assist Tomogr* 2007;31(3):348–353.
66. Raybaud C, Barkovich A. Intracranial, orbital, and neck masses of childhood. *Pediatric neuroimaging*. 5th ed. Philadelphia, Pa: Lippincott Williams & Wilkins, 2012; 684–687.
67. Luzzi S, Elia A, Del Maestro M, et al. Dysembryoplastic Neuroepithelial Tumors: What You Need to Know. *World Neurosurg* 2019;127:255–265.
68. Huse JT, Edgar M, Halliday J, Mikolaenko I, Lavi E, Rosenblum MK. Multinodular and vacuolating neuronal tumors of the cerebrum: 10 cases of a distinctive seizure-associated lesion. *Brain Pathol* 2013;23(5):515–524.
69. Nunes RH, Hsu CC, da Rocha AJ, et al. Multinodular and Vacuolating Neuronal Tumor of the Cerebrum: A New “Leave Me Alone” Lesion with a Characteristic Imaging Pattern. *AJNR Am J Neuroradiol* 2017;38(10):1899–1904.
70. Pajtlér KW, Witt H, Sill M, et al. Molecular Classification of Ependymal Tumors across All CNS Compartments, Histopathological Grades, and Age Groups. *Cancer Cell* 2015;27(5):728–743.
71. Nowak J, Jünger ST, Huflage H, et al. MRI Phenotype of RELA-fused Pediatric Supratentorial Ependymoma. *Clin Neuroradiol* 2019;29(4):595–604.
72. Andreiulo F, Varlet P, Tauziède-Espariat A, et al. Childhood supratentorial ependymomas with YAP1-MAMLD1 fusion: an entity with characteristic clinical, radiological, cytogenetic and histopathological features. *Brain Pathol* 2019;29(2):205–216.
73. Ramaswamy V, Hielscher T, Mack SC, et al. Therapeutic Impact of Cytoreductive Surgery and Irradiation of Posterior Fossa Ependymoma in the Molecular Era: A Retrospective Multicohort Analysis. *J Clin Oncol* 2016;34(21):2468–2477.
74. Mack SC, Witt H, Piro RM, et al. Epigenomic alterations define lethal CLMP-positive ependymomas of infancy. *Nature* 2014;506(7489):445–450.
75. Panwalkar P, Clark J, Ramaswamy V, et al. Immunohistochemical analysis of H3K27me3 demonstrates global reduction in group-A childhood posterior fossa ependymoma and is a powerful predictor of outcome. *Acta Neuropathol (Berl)* 2017;134(5):705–714.
76. Pajtlér KW, Wen J, Sill M, et al. Molecular heterogeneity and CXorf67 alterations in posterior fossa group A (PFA) ependymomas. *Acta Neuropathol (Berl)* 2018;136(2):211–226.
77. Witt H, Mack SC, Ryzhova M, et al. Delineation of two clinically and molecularly distinct subgroups of posterior fossa ependymoma. *Cancer Cell* 2011;20(2):143–157.
78. Yonezawa U, Karlowee V, Amartya VJ, et al. Radiology Profile as a Potential Instrument to Differentiate Between Posterior Fossa Ependymoma (PF-EPN) Group A and B. *World Neurosurg* 2020;140:e320–e327.
79. Träger M, Schweizer L, Pérez E, et al. Adult intracranial ependymoma-relevance of DNA methylation profiling for diagnosis, prognosis, and treatment. *Neuro Oncol* 2023;25(7):1286–1298.
80. Sharma T, Schwalbe EC, Williamson D, et al. Second-generation molecular subgrouping of medulloblastoma: an international meta-analysis of Group 3 and Group 4 subtypes. *Acta Neuropathol (Berl)* 2019;138(2):309–326.
81. Cavalli FMG, Remke M, Rampasek L, et al. Intertumoral Heterogeneity within Medulloblastoma Subgroups. *Cancer Cell* 2017;31(6):737–754.e6.
82. Coltin H, Sundaresan L, Smith KS, et al. Subgroup and subtype-specific outcomes in adult medulloblastoma. *Acta Neuropathol (Berl)* 2021;142(5):859–871.
83. Patay Z, DeSain LA, Hwang SN, Coan A, Li Y, Ellison DW. MR Imaging Characteristics of Wingless-Type-Subgroup Pediatric Medulloblastoma. *AJNR Am J Neuroradiol* 2015;36(12):2386–2393.
84. Phoenix TN, Patmore DM, Boop S, et al. Medulloblastoma Genotype Dictates Blood Brain Barrier Phenotype. *Cancer Cell* 2016;29(4):508–522.
85. Stock A, Mynarek M, Pietsch T, et al. Imaging Characteristics of Wingless Pathway Subgroup Medulloblastomas: Results from the German HIT/SIOP-Trial Cohort. *AJNR Am J Neuroradiol* 2019;40(11):1811–1817.
86. Yeom KW, Mobley BC, Lober RM, et al. Distinctive MRI features of pediatric medulloblastoma subtypes. *AJR Am J Roentgenol* 2013;200(4):895–903.
87. Perreault S, Ramaswamy V, Achrol AS, et al. MRI surrogates for molecular subgroups of medulloblastoma. *AJNR Am J Neuroradiol* 2014;35(7):1263–1269.
88. Keil VC, Warmuth-Metz M, Reh C, et al. Imaging Biomarkers for Adult Medulloblastomas: Genetic Entities May Be Identified by Their MR Imaging Radiophenotype. *AJNR Am J Neuroradiol* 2017;38(10):1892–1898.
89. Ramaswamy V, Remke M, Bouffet E, et al. Recurrence patterns across medulloblastoma subgroups: an integrated clinical and molecular analysis. *Lancet Oncol* 2013;14(12):1200–1207.